Supplemental Table S1. List of 404 Kinases Analyzed by AlphaScreen

#	Kinases	Value	#	Kinases	Value	#	Kinases	Value	#	Kinases	Value
1	PIM1	24020	36	MLKL	2880	71	DCAMKL1	1674	106	CDKL2	1184
2	LYN	22342	37	CK1g2	2602	72	MAPKAPK2	1668	107	CDK5	1180
3	ULK4	21784	38	CDKL3	2584	73	JAK3	1664	108	YANK2	1172
4	Fused	18910	39	CK1g1	2560	74	PAK1	1652	109	STLK6	1162
5	TGFbR1	15634	40	SgK495	2558	75	CK1d	1608	110	AMPKa2	1148
6	MLK1	12242	41	CK2a1	2534	76	FGR	1602	111	MNK2	1144
7	smMLCK	10084	42	PRPK	2528	77	CaMKK2	1578	112	TYRO3	1140
8	PDHK2	8868	43	GSK3B	2410	78	SYK	1576	113	RIOK2	1116
9	TSSK2	8310	44	PITSLRE	2304	79	LOK	1554	114	MST3	1114
10	HCK	8250	45	ULK3	2262	80	SgK223	1548	115	PKD2	1080
11	PIM2	7340	46	MAP2K2	2254	81	TSSK4	1546	116	MASTL	1066
12	DYRK3	5116	47	CK1g3	2218	82	SGK2	1530	117	MYO3A	1058
13	CK2a2	5068	48	ULK2	2212	83	SRPK1	1526	118	CASK	1056
14	JNK1	5048	49	MAP2K6	2112	84	RSK2	1496	119	RIPK1	1054
15	NEK7	5006	50	OSR1	2108	85	MNK1	1458	120	LATS2	1044
16	FGFR2	4930	51	NRBP1	2076	86	BMPR1A	1444	121	ILK	1040
17	TLK2	4716	52	LIMK2	2036	87	PINK1	1440	122	TIF1a	1038
18	Wee1B	4606	53	CHED	2018	88	Slob	1418	123	PKCa	1032
19	RSKL2	4552	54	CK1e	2012	89	SGK3	1400	124	DAPK1	1026
20	ROCK1	4502	55	RNAseL	1934	90	MAP2K1	1386	125	HIPK2	1022
21	HUNK	4448	56	FRAP	1932	91	FAK	1364	126	JAK1	1014
22	PKG2	4206	57	FER	1862	92	MAP3K2	1358	127	CaMK2g	992
23	FES	3900	58	PKACb	1854	93	CK1a	1354	128	JNK2	972
24	SGK	3782	59	DDR1	1846	94	ADCK1	1344	129	TIE1	966
25	HIPK1	3638	60	CaMK2b	1828	95	CDK8	1302	130	PKD3	954
26	MELK	3600	61	p70S6K	1824	96	ZC1/HGK	1262	131	Erk2	932
27	MARK3	3414	62	CaMK1a	1772	97	NIM1	1252	132	NIK	924
28	RET	3380	63	RSK1	1758	98	PHKg1	1248	133	NEK11	920
29	ADCK3	3380	64	Erk3	1744	99	PDGFRb	1244	134	Trb1	916
30	VRK1	3348	65	SCYL2	1740	100	ALK2	1238	135	MAP3K4	914
31	TAK1	3304	66	RIPK2	1692	101	MYT1	1236	136	KHS2	914
32	PLK1	3230	67	BUB1	1692	102	PKCd	1218	137	PDGFRa	912
33	PKN2	3152	68	p38a	1684	103	CLIK1	1218	138	NEK6	904
34	KIS	3126	69	skMLCK	1678	104	Trad	1204	139	FLT1	902
35	AurB	3102	70	ARAF	1676	105	AKT2	1198	140	AKT1	898

Supplemental Table S1. List of 404 Kinases Analyzed by AlphaScreen

#	Kinases	Value	#	Kinases	Value	#	Kinases	Value	#	Kinases	Value
141	BRD2	886	176	TESK1	740	211	SPEG	610	246	SRPK2	532
142	MOK	874	177	CSK	740	212	CaMK2d	610	247	PKCh	530
143	ROR2	870	178	SgK288	726	213	YES	608	248	IRR	530
144	GCN2	864	179	FLT3	710	214	PCTAIRE2	606	249	IRAK2	530
145	SCYL3	858	180	CDK3	710	215	LCK	600	250	TXK	528
146	CDKL1	854	181	IKKe	706	216	EphA7	598	251	AlphaK3	526
147	SRC	840	182	CDK4	706	217	CDK2	598	252	BARK2	516
148	DYRK1B	836	183	PDHK3	704	218	GPRK4	596	253	JAK2	510
149	CaMK1g	834	184	PIK3R4	702	219	PKCb	594	254	p38b	508
150	PAK2	822	185	TRKB	700	220	BLK	594	255	FYN	508
151	PKR	812	186	CDK10	700	221	STLK5	590	256	NEK1	506
152	PDHK4	812	187	IRAK3	696	222	TIF1b	584	257	NDR1	506
153	caMLCK	812	188	CLK4	694	223	LRRK2	584	258	PHKg2	500
154	IRAK1	806	189	MAK	690	224	DAPK3	584	259	CLK2	500
155	CTK	806	190	BMPR1B	690	225	VRK3	582	260	DDR2	498
156	JNK3	802	191	MUSK	688	226	TSSK1	576	261	TNK1	496
157	RYK	798	192	KDR	688	227	CRIK	576	262	p70S6Kb	496
158	HER4/ErbB4	794	193	PKCe	678	228	ULK1	572	263	TAO3	494
159	MST2	788	194	BARK1	678	229	TESK2	572	264	MLK2	494
160	MAP3K3	788	195	SgK196	668	230	PKN1	572	265	NEK5	492
161	DYRK1A	784	196	ACTR2	664	231	PKCg	570	266	CCRK	492
162	eEF2K	778	197	PRKX	658	232	EphA3	570	267	CaMKK1	490
163	CHK1	774	198	p38g	658	233	ALK4	564	268	BMX	484
164	DAPK2	772	199	MSK2	652	234	A6r	564	269	PAK5	474
165	RIPK3	770	200	INSR	652	235	EphA1	562	270	TTBK1	470
166	DCAMKL3	766	201	MAPKAPK5	644	236	EphB4	558	271	Trb3	470
167	SgK269	762	202	TBCK	642	237	ZAP70	556	272	G11	466
168	CDKL5	762	203	HER3/ErbB3	640	238	H11	552	273	IKKb	464
169	TYK2	760	204	TTK	638	239	GPRK5	548	274	CaMK2a	464
170	NuaK2	760	205	TAO2	638	240	COT	546	275	Trb2	462
171	IKKa	758	206	STK33	628	241	NDR2	542	276	EphA4	462
172	RSK4	756	207	SNRK	622	242	DRAK1	542	277	DYRK2	460
173	DNAPK	750	208	MST1	620	243	HRI	538	278	TRKA	458
174	YSK1	748	209	TRKC	614	244	MAPKAPK3	536	279	FGFR1	458
175	RSK3	742	210	FRK	612	245	AurC	534	280	MAP3K6	456

Supplemental Table S1. List of 404 Kinases Analyzed by AlphaScreen

#	Kinases	Value	#	Kinases	Value	#	Kinases	Value	#	Kinases	Value
281	SgK496	454	312	ANKRD3	396	343	PIM3	352	374	DCAMKL2	284
282	KSR1	454	313	BCKDK	394	344	ITK	352	375	GCK	282
283	CLK1	454	314	CDK6	392	345	CDK11	350	376	PRP4	280
284	IRE2	452	315	ADCK4	390	346	CDC2	348	377	MLK4	274
285	TSSK3	446	316	TBK1	388	347	ABL	346	378	GPRK6	274
286	CYGD	438	317	CaMK1b	388	348	PAK6	344	379	DLK	272
287	PKCt	436	318	SuRTK106	386	349	MARK1	344	380	PSKH1	270
288	PCTAIRE3	432	319	PKG1	386	350	FGFR3	342	381	NEK2	268
289	AlphaK1	432	320	PFTAIRE1	386	351	BUBR1	342	382	AXL	268
290	EphB1	430	321	NEK8	386	352	p38d	340	383	CDK9	266
291	MET	428	322	ROR1	382	353	MST4	338	384	Erk4	264
292	IRE1	428	323	LMR1	382	354	CaMK4	336	385	PYK2	262
293	MARK2	424	324	GAK	382	355	AMPKa1	334	386	ALK7	260
294	CCK4	424	325	SCYL1	380	356	NEK4	332	387	PDK1	256
295	ZAK	422	326	MAP3K7	378	357	BRK	332	388	PASK	256
296	HER2/ErbB2	420	327	IGF1R	372	358	EphA6	330	389	EphA2	256
297	EphB6	420	328	AurA	370	359	TIE2	324	390	MAST2	254
298	BIKE	420	329	SSTK	368	360	PAK3	324	391	MPSK1	252
299	FASTK	418	330	RSKL1	368	361	MARK4	324	392	CDK7	252
300	BRD3	416	331	GSK3A	366	362	PCTAIRE1	320	393	SIK	250
301	LIMK1	414	332	MAP2K5	364	363	MAP2K3	320	394	DRAK2	250
302	HIPK3	414	333	FMS	364	364	EphA5	320	395	YANK3	244
303	VRK2	408	334	MAST4	362	365	PKCz	318	396	PAK4	244
304	HSER	408	335	FGFR4	362	366	TEC	312	397	KHS1	244
305	QIK	406	336	EphB3	360	367	A6	310	398	ZC2/TNIK	240
306	CaMK1d	406	337	TLK1	358	368	RIOK3	304	399	RIOK1	240
307	RON	404	338	CHK2	358	369	STLK3	298	400	MAP2K7	240
308	FLT4	402	339	ACTR2B	358	370	Erk5	296	401	PFTAIRE2	236
309	CLK3	402	340	PEK	356	371	PKCi	290	402	MYO3B	224
310	RAF1	400	341	PDHK1	356	372	PBK	284	403	MAP2K4	218
311	ICK	398	342	TGFbR2	352	373	IRAK4	284	404	KIT	216

Footnotes.

- Kinases are sorted in descending order (largest value first) according to AlphaScreen values.
- Data shown are mean values of duplicate experiments.

Supplemental Table S2.
Serine/Threonine Kinases Analyzed by *In Vitro* Phosphorylation Assay

		Relative Kinase Activity				Relative Kinase Activity	
Kinases	LU	FL	D3	Kinases	LU	FL	D3
PIM1	24020	1.77	4.06	CKI-γ1	2560	n/a*	138.69
ULK4	21784	1.02	0.79	PRPK	2528	1.57	3.04
Fused	18910	0.84	0.92	GSK3B	2410	1.53	1.58
TGFβR1	15634	1.10	2.12	PITSLRE	2304	2.26	2.94
MLK1	12242	2.69	0.64	CKI-γ3	2218	0.23	52.51
smMLCK	10084	1.41	0.92	MAP2K6	2112	n/a	0.14
PDHK2	8868	0.91	2.54	NRBP1	2076	n/a	0.97
TSSK2	8310	4.24	14.94	LIMK2	2036	0.80	0.47
PIM2	7340	0.95	1.00	CHED	2018	n/a	1.50
DYRK3	5116	1.62	0.99	CKI-ε	2012	7.95	9.48
CKII-α'	5068	2.30	8.20	RNAseL	1934	n/a	1.15
JNK1	5048	0.64	1.95	FRAP	1932	n/a	1.30
NEK7	5006	1.69	1.52	PKACβ	1854	0.15	69.54
TLK2	4716	1.27	0.96	CaMK2β	1828	1.53	0.97
Wee1B	4606	1.27	2.62	RSK1	1758	0.78	0.55
RSKL2	4552	n/a	1.27	Erk3	1744	n/a	1.63
ROCK1	4502	n/a*	1.26	BUB1	1692	1.02	0.95
HUNK	4448	1.67	1.00	p38α	1684	n/a	1.01
PKG2	4206	0.22	2.44	skMLCK	1678	n/a	1.45
SGK	3782	2.28	1.19	DCAMKL1	1674	n/a	5.55
MARK3	3414	n/a	4.48	MAPKAPK2	1668	1.39	1.63
ADCK3	3380	n/a	1.49	CaMKK2	1578	n/a	3.49
VRK1	3348	2.41	1.75	SGK2	1530	n/a	1.26
Plk1	3230	2.70	44.65	MNK1	1458	1.69	2.84
PKN2	3152	0.80	1.99	Slob	1418	n/a	0.63
KIS	3126	3.36	1.11	MAP3K2	1358	n/a	1.22
CKI-γ2	2602	4.31	3.15	CKI-α	1354	4.66	1.00
CDKL3	2584	0.98	3.09				

Footnotes. LU: light unit in AlphaScreen; FL: full-length NS5A; D3: domain III of NS5A; n/a: not assessed due to low amounts of full-length NS5A; n/a*: not assessed due to overlap between purified kinases and NS5A on the gel; Relative Kinase Activity: fold increase of the *in vitro* kinase activity of each kinase relative to that of DHFR.

Supplemental Table S3. NS5A Peptides Identified by LC-MS/MS

m/z	Mass	Charge State	Peptide Score	Peptide Sequence	Location in NS5A (aa)	Modification (Residue)	Knockdown	No. of Peptide
1196.5	3586.6	3	25.1	ATCTTHSNTYDVDMVDANLLMEGGVAQTEPESR	241 - 273	Oxidation (M)	Ctrl	1
1182.6	2363.2	2	31.5	LARGSPPSEASSSVSQLSAPSLR	218 - 240	Phosphorylation (S/T)	Ctrl	1
1182.6	2363.2	2	27.6	LARGSPPSEASSSVSQLSAPSLR	218 - 240	Phosphorylation (S/T)	CKI-α	1
1119.6	2237.1	2	27.3	ALPAWARPDYNPPLVESWR	308 - 326		Ctrl	1
1072.6	2143.2	2	63.4	RTVGLSESTISEALQQLAIK	355 - 374		Ctrl	5
1072.6	2143.2	2	99.2	RTVGLSESTISEALQQLAIK	355 - 374		CKI-α	3
1052.5	2102.9	2	25.0	GSPPSEASSSVSQLSAPSLR	221 - 240	Phosphorylation (S/T)	Ctrl	1
1034.5	2067.0	2	34.0	TVGLSESTISEALQQLAIK	356 - 374	Phosphorylation (S/T)	Ctrl	1
1012.5	2022.9	2	99.4	GSPPSEASSSVSQLSAPSLR	221 - 240	Phosphorylation (S/T)	Ctrl	8
1012.5	2022.9	2	96.2	GSPPSEASSSVSQLSAPSLR	221 - 240	Phosphorylation (S/T)	CKI-α	13
1012.5	2022.9	2	72.5	GSPPSEASSSVSQLSAPSLR	221 - 240	Phosphorylation (S/T)	Ctrl	2
1012.5	2022.9	2	70.8	GSPPSEASSSVSQLSAPSLR	221 - 240	Phosphorylation (S/T)	CKI-α	2
994.5	1987.1	2	123.0	TVGLSESTISEALQQLAIK	356 - 374		Ctrl	10
994.5	1987.1	2	107.0	TVGLSESTISEALQQLAIK	356 - 374		CKI-α	10
989.5	1977.0	2	65.0	RPDYQPPTVAGCALPPPK	327 - 344	Propionamide (C)	CKI-α	8
972.5	1943.0	2	122.3	GSPPSEASSSVSQLSAPSLR	221 - 240		Ctrl	48
972.5	1943.0	2	132.3	GSPPSEASSSVSQLSAPSLR	221 - 240		CKI-α	73
968.8	2903.4	3	60.7	VAASEYAEVTQHGSYSYVTGLTTDNLK	113 - 139		Ctrl	5
968.8	2903.4	3	70.2	VAASEYAEVTQHGSYSYVTGLTTDNLK	113 - 139		CKI-α	12
954.0	1906.0	2	59.0	RPDYQPPTVAGCALPPPK	327 - 344		CKI-α	8
863.9	1725.8	2	81.8	SMLTDPPHITAETAAR	201 - 216	Oxidation (M)	Ctrl	20
863.9	1725.8	2	87.0	SMLTDPPHITAETAAR	201 - 216	Oxidation (M)	CKI-α	75
855.9	1709.8	2	86.6	SMLTDPPHITAETAAR	201 - 216		Ctrl	23
855.9	1709.8	2	86.4	SMLTDPPHITAETAAR	201 - 216		CKI-α	17
842.8	2525.3	3	58.5	IPCQLPSPEFFSWVDGVQIHR	140 - 160	Propionamide (C)	Ctrl	2
842.8	2525.3	3	53.9	IPCQLPSPEFFSWVDGVQIHR	140 - 160	Propionamide (C)	CKI-α	1
819.1	2454.2	3	68.6	IPCQLPSPEFFSWVDGVQIHR	140 - 160		Ctrl	2
819.1	2454.2	3	53.2	IPCQLPSPEFFSWVDGVQIHR	140 - 160		CKI-α	1
799.4	1596.8	2	60.8	GYKGVWAGTGIMTTR	42 - 56		Ctrl	2
799.4	1596.8	2	72.0	GYKGVWAGTGIMTTR	42 - 56		CKI-α	2
794.1	2379.3	3	59.0	RRTVGLSESTISEALQQLAIK	354 - 374	Phosphorylation (S/T)	CKI-α	1
788.7	2363.1	3	46.0	LARGSPPSEASSSVSQLSAPSLR	218 - 240	Phosphorylation (S/T)	Ctrl	3
788.7	2363.1	3	54.4	LARGSPPSEASSSVSQLSAPSLR	218 - 240	Phosphorylation (S/T)	CKI-α	2
679.0	2034.1	3	75.4	RPDYQPPTVAGCALPPPKK	327 - 345		Ctrl	6
679.0	2034.1	3	83.9	RPDYQPPTVAGCALPPPKK	327 - 345		CKI-α	4
675.3	2022.9	3	36.9	GSPPSEASSSVSQLSAPSLR	221 - 240	Phosphorylation (S/T)	Ctrl	1
675.3	2022.9	3	25.0	GSPPSEASSSVSQLSAPSLR	221 - 240	Phosphorylation (S/T)	Ctrl	1
666.8	1331.6	2	67.7	CPCGANISGNVR	57 - 68	Propionamide (C)	Ctrl	2
666.8	1331.6	2	64.1	CPCGANISGNVR	57 - 68	Propionamide (C)	CKI-α	2
660.0	1977.0	3	74.2	RPDYQPPTVAGCALPPPK	327 - 344	Propionamide (C)	Ctrl	8
637.4	1272.7	2	44.4	LPGLPFISCQK	31 - 41	Propionamide (C)	Ctrl	4
637.4	1272.7	2	53.0	LPGLPFISCQK	31 - 41	Propionamide (C)	CKI-α	4
636.3	1906.0	3	68.9	RPDYQPPTVAGCALPPPK	327 - 344		Ctrl	13
633.3	1264.6	2	66.6	GVWAGTGIMTTR	45 - 56	Oxidation (M)	Ctrl	6
633.3	1264.6	2	64.4	GVWAGTGIMTTR	45 - 56	Oxidation (M)	CKI-α	8
631.3	1260.6	2	74.9	CPCGANISGNVR	57 - 68	Propionamide (C)	Ctrl	1
631.3	1260.6	2	55.5	CPCGANISGNVR	57 - 68	Propionamide (C)	CKI-α	1
631.3	1260.6	2	72.7	CPCGANISGNVR	57 - 68	Propionamide (C)	Ctrl	2
631.3	1260.6	2	61.2	CPCGANISGNVR	57 - 68	Propionamide (C)	CKI-α	2
625.3	1248.6	2	75.5	GVWAGTGIMTTR	45 - 56		Ctrl	71
625.3	1248.6	2	69.6	GVWAGTGIMTTR	45 - 56		CKI-α	42
604.3	1206.7	2	27.3	FAPTPKPFFR	161 - 170		CKI-α	2
601.8	1201.7	2	45.3	LPGLPFISCQK	31 - 41		Ctrl	6
601.8	1201.7	2	51.6	LPGLPFISCQK	31 - 41		CKI-α	5
595.8	1189.5	2	79.8	CPCGANISGNVR	57 - 68		Ctrl	9
595.8	1189.5	2	74.6	CPCGANISGNVR	57 - 68		CKI-α	11
550.3	1098.6	2	39.7	KAPTPPPRR	345 - 353	Phosphorylation (S/T)	Ctrl	10
550.3	1098.6	2	33.6	KAPTPPPRR	345 - 353	Phosphorylation (S/T)	CKI-α	8
510.3	1018.6	2	40.4	KAPTPPPRR	345 - 353		Ctrl	9
510.3	1018.6	2	28.8	KAPTPPPRR	345 - 353		CKI-α	4
472.2	942.5	2	45.1	KAPTPPPR	345 - 352	Phosphorylation (S/T)	Ctrl	6
472.2	942.5	2	30.7	KAPTPPPR	345 - 352	Phosphorylation (S/T)	CKI-α	6
446.3	890.5	2	31.4	APTPPPRR	346 - 353		CKI-α	1
432.3	862.5	2	35.3	KAPTPPPR	345 - 352		Ctrl	3
432.3	862.5	2	35.3	KAPTPPPR	345 - 352		CKI-α	2
374.7	747.4	2	25.8	NWLTSK	21 - 26		CKI-α	1
353.2	704.4	2	36.0	SGSWLR	1 - 6		Ctrl	2
353.2	704.4	2	43.0	SGSWLR	1 - 6		CKI-α	2
							Total	629

SUPPLEMENTAL TABLE S3. NS5A Peptides Identified by LC-MS/MS

Footnotes. *m/z*: mass-to-charge ratio; Mass: molecular weight of a peptide; Charge State: number of charges of peptide ions; Peptide Score: parameter for peptide selection, and a minimum peptide score of 25 is used in this study; No. of Peptide: number of peptides identified. Peptides #1, #2, and #3 are highlighted in green, blue, and yellow, respectively. Phosphopeptides are indicated in bold red letters. Modified amino acids are underlined.

Journal of General Virology (2014), 95, 2658–2667 DOI 10.1099/vir.0.068528-0

Alternative endocytosis pathway for productive entry of hepatitis C virus

Mami Matsuda,[1] Ryosuke Suzuki,[1] Chikako Kataoka,[1] Koichi Watashi,[1] Hideki Aizaki,[1] Nobuyuki Kato,[2] Yoshiharu Matsuura,[3] Tetsuro Suzuki[4] and Takaji Wakita[1]

Correspondence
Ryosuke Suzuki
ryosuke@niid.go.jp

[1]Department of Virology II, National Institute of Infectious Diseases, Tokyo, Japan

[2]Department of Tumor Virology, Okayama University Graduate School of Medicine, Dentistry, and Pharmaceutical Sciences, Okayama, Japan

[3]Research Institute for Microbial Diseases, Osaka University, Osaka, Japan

[4]Department of Infectious Diseases, Hamamatsu University School of Medicine, Shizuoka, Japan

Previous studies have shown that hepatitis C virus (HCV) enters human hepatic cells through interaction with a series of cellular receptors, followed by clathrin-mediated, pH-dependent endocytosis. Here, we investigated the mechanisms of HCV entry into multiple HCV-permissive human hepatocyte-derived cells using trans-complemented HCV particles (HCVtcp). Knockdown of CD81 and claudin-1, or treatment with bafilomycin A1, reduced infection in Huh-7 and Huh7.5.1 cells, suggesting that HCV entered both cell types via receptor-mediated, pH-dependent endocytosis. Interestingly, knockdown of the clathrin heavy chain or dynamin-2 (Dyn2), as well as expression of the dominant-negative form of Dyn2, reduced infection of Huh-7 cells with HCVtcp, whereas infectious entry of HCVtcp into Huh7.5.1 cells was not impaired. Infection of Huh7.5.1 cells with culture-derived HCV (HCVcc) via a clathrin-independent pathway was also observed. Knockdown of caveolin-1, ADP-ribosylation factor 6 (Arf6), flotillin, p21-activated kinase 1 (PAK1) and the PAK1 effector C-terminal binding protein 1 of E1A had no inhibitory effects on HCVtcp infection into Huh7.5.1 cells, thus suggesting that the infectious entry pathway of HCV into Huh7.5.1 cells was not caveolae-mediated, or Arf6- and flotillin-mediated endocytosis and macropinocytosis, but rather may have occurred via an undefined endocytic pathway. Further analysis revealed that HCV entry was clathrin- and dynamin-dependent in ORL8c and HepCD81/miR122 cells, but productive entry of HCV was clathrin- and dynamin-independent in Hep3B/miR122 cells. Collectively, these data indicated that HCV entered different target cells through different entry routes.

Received 29 May 2014
Accepted 1 August 2014

INTRODUCTION

Over 170 million people worldwide are chronically infected with hepatitis C virus (HCV), and are at risk of developing chronic hepatitis, cirrhosis and hepatocellular carcinoma (Hoofnagle, 2002). HCV is an enveloped virus belonging to the family *Flaviviridae*. Its genome is an uncapped 9.6 kb positive-stranded RNA consisting of the 5′-UTR, an ORF encoding viral proteins and the 3′-UTR (Suzuki *et al.*, 2007). A precursor polyprotein is further processed into structural proteins (core, E1, and E2), followed by p7 and non-structural (NS) proteins (NS2, NS3, NS4A, NS4B, NS5A and NS5B), by cellular and viral proteases.

Two supplementary figures are available with the online version of this paper.

Host–virus interactions are required during the initial steps of viral infection. Viruses enter the cells by various pathways, such as receptor-mediated endocytosis followed by pH-dependent or -independent fusion from endocytic compartments, or pH-independent fusion at the plasma membrane coupled with receptor-mediated signalling and coordinated disassembly of the actin cortex (Grove & Marsh, 2011). It was reported previously that CD81 (Bartosch *et al.*, 2003; McKeating *et al.*, 2004; Pileri *et al.*, 1998), scavenger receptor class B type I (SR-BI) (Bartosch *et al.*, 2003; Scarselli *et al.*, 2002), claudin-1 (Evans *et al.*, 2007; Liu *et al.*, 2009) and occludin (Benedicto *et al.*, 2009; Liu *et al.*, 2009; Ploss *et al.*, 2009) are critical molecules for HCV entry into cells. Recently, epidermal growth factor receptor and ephrin receptor type A2 were also identified as host cofactors for HCV entry, possibly by modulating interactions between CD81 and claudin-1 (Lupberger *et al.*,

2011). In addition, Niemann–Pick C1-like 1 (NPC1L1) cholesterol absorption receptor has been shown to play a role in HCV entry, probably at the fusion step (Sainz *et al.*, 2012).

Following receptor binding, HCV has been reported to enter cultured cells via clathrin-mediated endocytosis, the most common and best-characterized mode of endocytosis, following membrane fusion in early endosomes (Blanchard *et al.*, 2006; Codran *et al.*, 2006; Coller *et al.*, 2009; Meertens *et al.*, 2006; Trotard *et al.*, 2009) using retrovirus-based HCV pseudoparticles (HCVpp) and cell culture-produced HCV (HCVcc). Early steps in HCV infection, including the role of HCV glycoprotein heterodimers, receptor binding, internalization and pH-dependent endosomal fusion, have been at least in part mimicked by HCVpp. However, as HCVpp are generated in non-hepatic cells such as human embryo kidney 293T cells, it is likely that the cell-derived component(s) of HCVpp differ from those of HCVcc.

In the present study, we readdressed the HCV endocytosis pathway using trans-complemented HCV particles (HCVtcp) (Suzuki *et al.*, 2012), of which the packaged genome is a subgenomic replicon. HCVtcp, generated in Huh-7 or its derivative cell lines with two plasmids, are infectious, but support only single-round infection, thereby allowing us to examine infectious viral entry without the influence of reinfection. In addition, HCVtcp is useful for quantifying productive infection by measuring luciferase activity. Furthermore, it has been shown that the HCVtcp system is more relevant as a model of HCV infection than HCVpp (Suzuki *et al.*, 2012). Our results demonstrated conclusively that, in addition to the clathrin-mediated endocytosis pathway, HCV was capable of utilizing the clathrin- and dynamin-independent pathways for infectious entry of HCV into human liver-derived cells.

RESULTS

HCV entry depends on receptor-mediated, pH-dependent endocytosis

HCV has been shown to enter permissive cells through clathrin-mediated endocytosis and low pH-dependent fusion with endosomes mostly using HCVpp (Codran *et al.*, 2006; Meertens *et al.*, 2006; Trotard *et al.*, 2009), although some researchers have used HCVcc with limited cell lines (Blanchard *et al.*, 2006; Coller *et al.*, 2009). However, several distinct characteristics between HCVpp and HCVcc have recently been revealed with regard to morphogenesis and entry steps (Helle *et al.*, 2010; Sainz *et al.*, 2012; Suzuki *et al.*, 2012; Vieyres *et al.*, 2010). Therefore, in this study, we used HCVtcp, which exhibit similar characteristics to HCVcc when compared with HCVpp and support single-round infection (Suzuki *et al.*, 2012).

Initially, to determine whether receptor candidates such as CD81, claudin-1, occludin and SR-BI are essential for HCV entry into Huh-7 and Huh7.5.1 cells, we examined the knockdown effect of these molecules on HCVtcp infection. Knockdown of these receptors was confirmed by immunoblotting (Fig. 1a) and FACS analysis (Fig. 1b). It should be noted that the luciferase activity in Huh7.5.1 was approximately four times higher than that in Huh-7 cells when the same amount of inoculum was used for infection (Fig. S1, available in the online Supplementary Material), and knockdown did not affect cell viability (data not shown). Knockdown of CD81 and claudin-1 significantly reduced the infection of Huh-7 and Huh7.5.1 cells with HCVtcp derived from genotype 2a (Fig. 1c). Knockdown of occludin led to a moderate reduction in infection; however, only a marginal effect was observed in SR-BI knockdown in both Huh-7 and Huh7.5.1 cells (Fig. 1c), possibly due to the reduced requirement for SR-BI during virus entry by adaptive mutation in E2 (Grove *et al.*, 2008).

Next, to examine whether HCV entry was pH-dependent, Huh-7 and Huh7.5.1 cells were pretreated with bafilomycin A1, an inhibitor of vacuolar H^+-ATPases that impairs vesicle acidification, and then infected with HCVtcp. At 72 h post-infection, luciferase activity and cell viability were determined. Bafilomycin A1 inhibited HCVtcp infection in a dose-dependent manner without affecting cell viability in both Huh-7 and Huh7.5.1 cells (Fig. 2a, b). We also confirmed that treatment with bafilomycin A1 after HCVtcp infection had a minor effect on luciferase activity (Fig. 2c). These results indicated that the infectious route of HCVtcp into Huh-7 and Huh7.5.1 cells is receptor-mediated and involves pH-dependent endocytosis.

Knockdown of clathrin heavy chain (CHC) or dynamin-2 (Dyn2) reduces HCVtcp infection in Huh-7 cells, but not in Huh7.5.1 cells

Among the known pathways of pH-dependent viral endocytosis, clathrin-mediated dynamin-dependent endocytosis is a major endocytosis pathway. Chlorpromazine, an inhibitor of clathrin-dependent endocytosis, has been commonly used to study clathrin-mediated endocytosis; however, it exerts multiple side-effects on cell function as it targets numerous receptors and intracellular enzymes, and alters plasma membrane characteristics (Sieczkarski & Whittaker, 2002a). Therefore, we examined the HCV endocytosis pathway by knockdown of specific molecules required for the endocytosis pathway. CHC, a major structural protein in clathrin-coated vesicles, and Dyn2, a GTPase essential for clathrin-coated-pit scission from the plasma membrane, play important roles in the clathrin-mediated pathway. Another well-studied model of viral entry is caveolin-mediated endocytosis. The role of dynamin in both clathrin-mediated endocytosis and caveolae-dependent endocytosis has been established (Marsh & Helenius, 2006; Miaczynska & Stenmark, 2008). To examine the endocytosis pathways of HCV, small interfering RNAs (siRNAs) for CHC, Dyn2 and caveolin-1 (Cav1), or scrambled control siRNA, were transfected into Huh-7 or

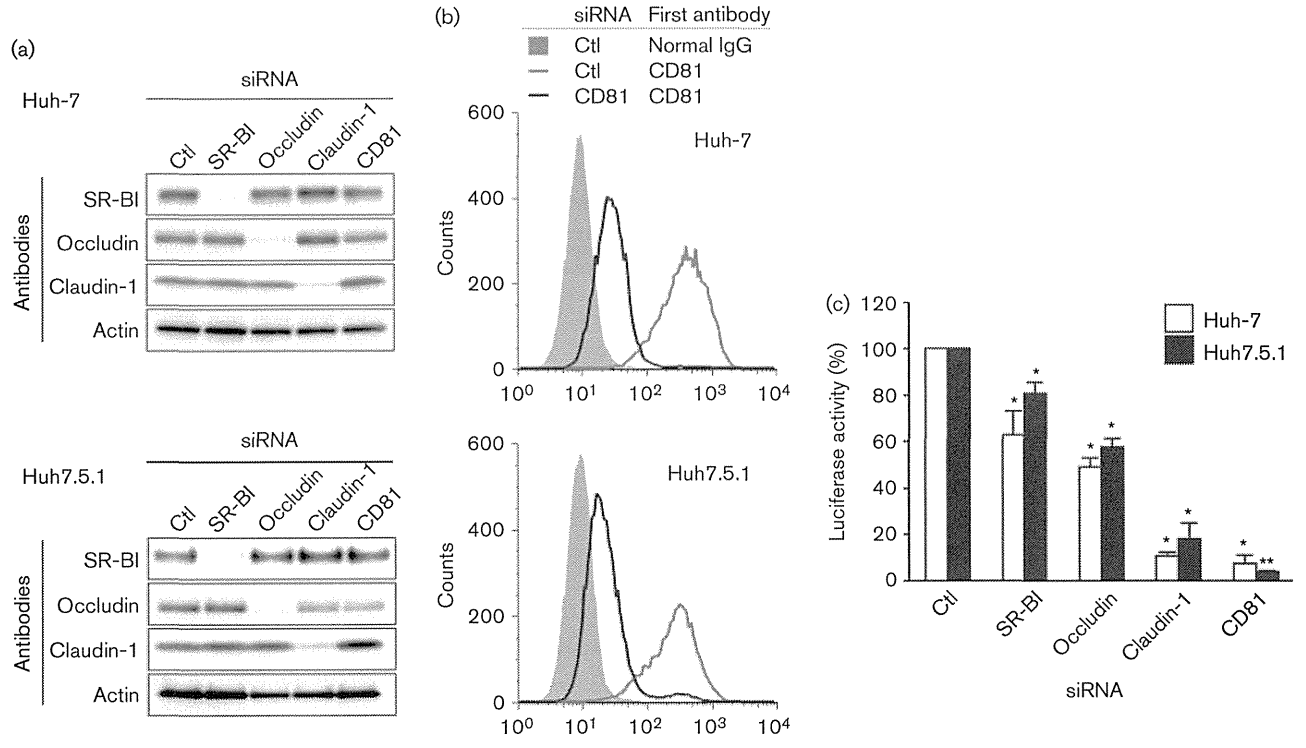

Fig. 1. Knockdown effect of receptor candidate molecules on HCV infection. (a) Huh-7 or Huh7.5.1 cells were transfected with the indicated small interfering RNAs (siRNA), harvested at 48 h post-transfection and the specific knockdown of each protein was verified by immunoblotting. (b) Huh-7 or Huh7.5.1 cells were transfected with CD81 or control siRNAs, harvested at 48 h post-transfection and the cell surface expression of CD81 was verified by FACS analysis. (c) Cells transfected with siRNA were infected with the same amount of HCVtcp at 48 h post-transfection. Firefly luciferase activity in the cells was determined at 72 h post-infection and is expressed relative to the activity with control siRNA transfection. The value for control (Ctl) siRNA was set at 100 %. Data represent the mean ± SD. Statistical differences between controls and each siRNA were evaluated using Student's *t*-test. **P*<0.05, ***P*<0.001 versus control.

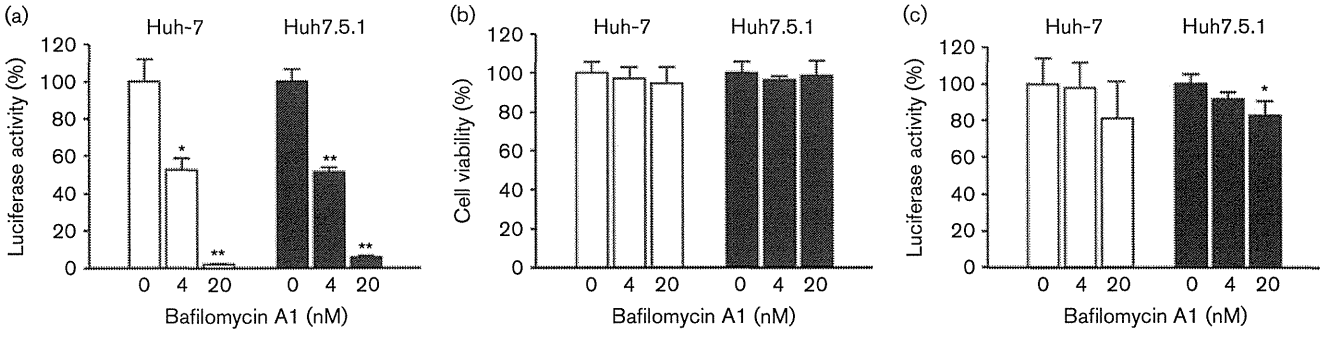

Fig. 2. Role of endosomal low pH in HCV infection. Cells were treated with bafilomycin A1 for 1 h at the indicated concentrations and infected with HCVtcp. (a, b) Luciferase activity (a) and cell viability (b) were determined at 72 h post-infection, and expressed relative to amounts observed in controls. (c) Cells were treated with bafilomycin A1 for 1 h at the indicated concentrations 48 h after HCVtcp infection. Luciferase activity was determined at 10 h post-treatment and expressed relative to amounts observed in controls. Data represent the mean ± SD. Statistical differences between controls and indicated concentrations were evaluated using Student's *t*-test. **P*<0.05, ***P*<0.001 versus control.

Huh7.5.1 cells, followed by infection with HCVtcp. Expression of CHC, Dyn2 and Cav1 was downregulated by transfection of specific siRNAs (Fig. 3a, b), whereas expression of SR-BI, occludin, claudin-1 and CD81 was not reduced (Figs 3a and S2). As indicated in Fig. 3(c), luciferase activity from HCVtcp was significantly reduced by knockdown of CHC and Dyn2 in Huh-7 cells, but not in Huh7.5.1 cells. Knockdown of Cav1 showed no inhibitory effects on HCVtcp entry into either cell line. Dynamin-independent entry in Huh7.5.1 cells was also observed using HCVtcp derived from genotype 1b (data not shown). Knockdown of CHC or Dyn2 also reduced entry of HCVcc in Huh-7 cells, but had no inhibitory effects in Huh7.5.1 (Fig. 3d). To rule out the possibility of effects on CHC and Dyn2 knockdown on viral RNA replication, HCVtcp were also inoculated before siRNA transfection. Luciferase activity was not affected by knockdown of CHC or Dyn2 in either cell line, whereas marked inhibition was observed for phosphatidylinositol 4-kinase (PI4K) (Fig. 3e). These data suggested that HCV entry was clathrin-mediated and dynamin-dependent in Huh-7 cells, but productive entry of HCV was clathrin- and dynamin-independent in Huh7.5.1 cells.

Expression of the dominant-negative form of Dyn2 reduces HCV infection in Huh-7 cells, but not in Huh7.5.1 cells

We also examined the role of dynamin in infectious entry of HCV into Huh-7 and Huh7.5.1 cells by overexpression of the dominant-negative form of Dyn2 (Dyn-K44A), which

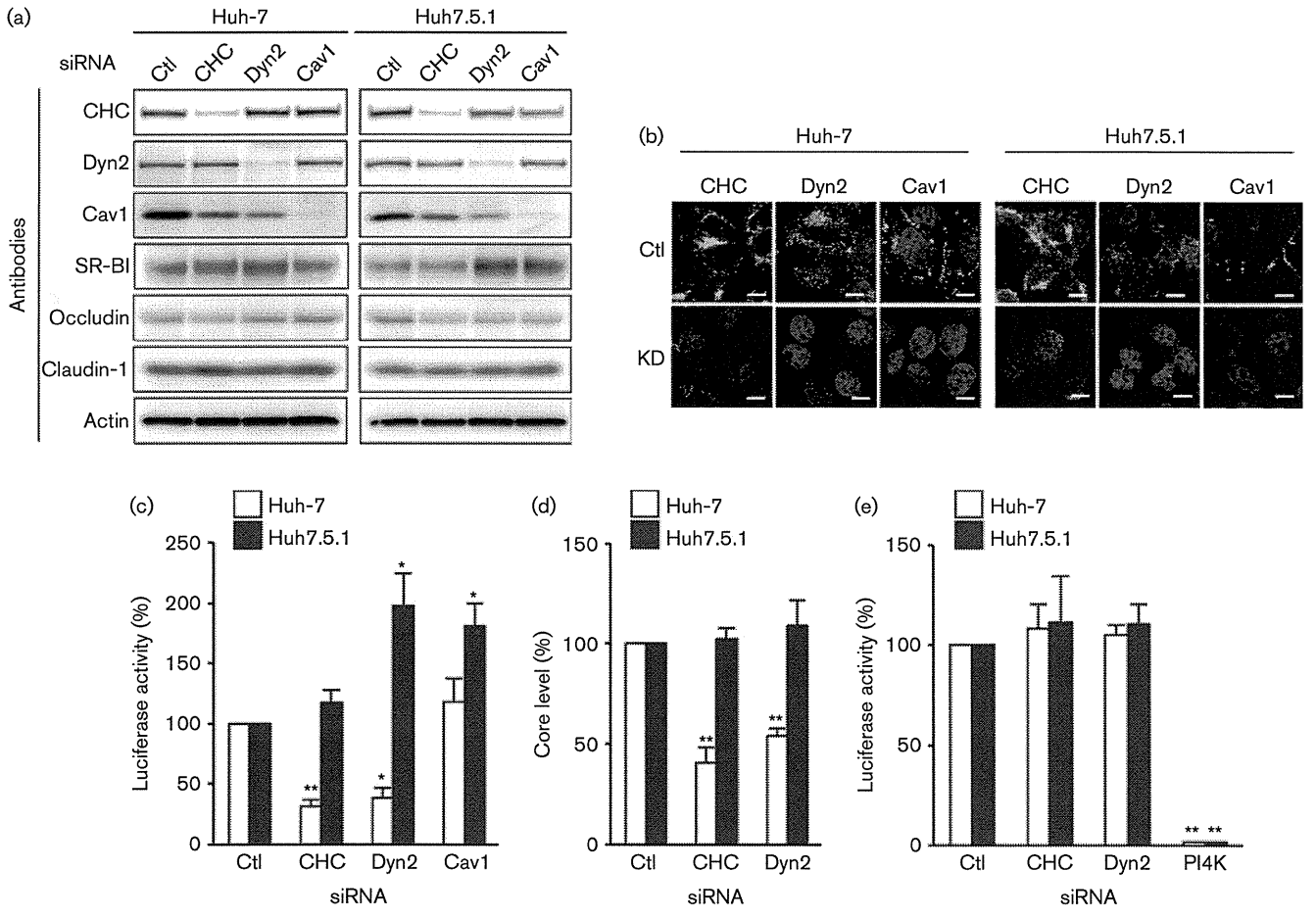

Fig. 3. Effects of CHC, Dyn2 and Cav1 knockdown on HCV infection. (a, b) Huh-7 cells or Huh7.5.1 cells were transfected with the indicated siRNAs and the specific knockdown (KD) of each protein was verified by immunoblotting (a) or immunostaining (b) at 48 h post-transfection. Bar, 50 μm. (c) Cells were transfected with the indicated siRNAs, followed by infection with HCVtcp at 48 h post-transfection. Firefly luciferase activity in the cells was subsequently determined at 3 days post-infection. The value for control (Ctl) siRNA was set at 100 %. Data represent the mean ± SD. (d) Cells were transfected with siRNA, followed by infection with HCVcc at 48 h post-transfection. Intracellular core levels were quantified at 24 h post-infection. The value for control siRNA was set at 100 %. Data represent the mean ± SD. (e) Cells were infected with HCVtcp, followed by transfection with the indicated siRNAs. Luciferase activity in the cells was subsequently determined at 2 days post-transfection. The value for control siRNA was set at 100 %. Data represent the mean ± SD. Statistical differences between controls and each siRNA were evaluated using Student's *t*-test. **P*<0.05, ***P*<0.001 versus control.

has been shown to effectively block clathrin-dependent and caveolar endocytosis (Damke *et al.*, 1995). Expression of haemagglutinin (HA)-tagged Dyn-K44A reduced the number of HCV-infected Huh-7 cells, but not Huh7.5.1 cells, as compared with WT HA-tagged Dyn2 (Dyn-WT), as shown in Fig. 4(a, b). Interestingly, internalization of transferrin, which is known to be mediated by clathrin-dependent endocytosis, was reduced in both Huh-7 and Huh7.5.1 cells expressing Dyn-K44A, whereas cells expressing Dyn-WT showed efficient endocytosis of transferrin (Fig. 4c, d). Collectively, these results suggested that dynamin participated in the internalization of HCV in Huh-7 cells, but was not absolutely required in Huh7.5.1 cells, although transferrin was taken up via dynamin-dependent endocytosis in both Huh-7 and Huh7.5.1 cells.

Flotillin-1 or the GTPase regulator associated with focal adhesion kinase 1 (GRAF1) play no major role during HCV infection of Huh7.5.1 cells

In order to dissect the major endocytosis pathways of HCVtcp in Huh7.5.1 cells, we investigated the role of alternative routes of HCV entry by siRNA knockdown. We silenced essential factors for the clathrin- or dynamin-independent pathways

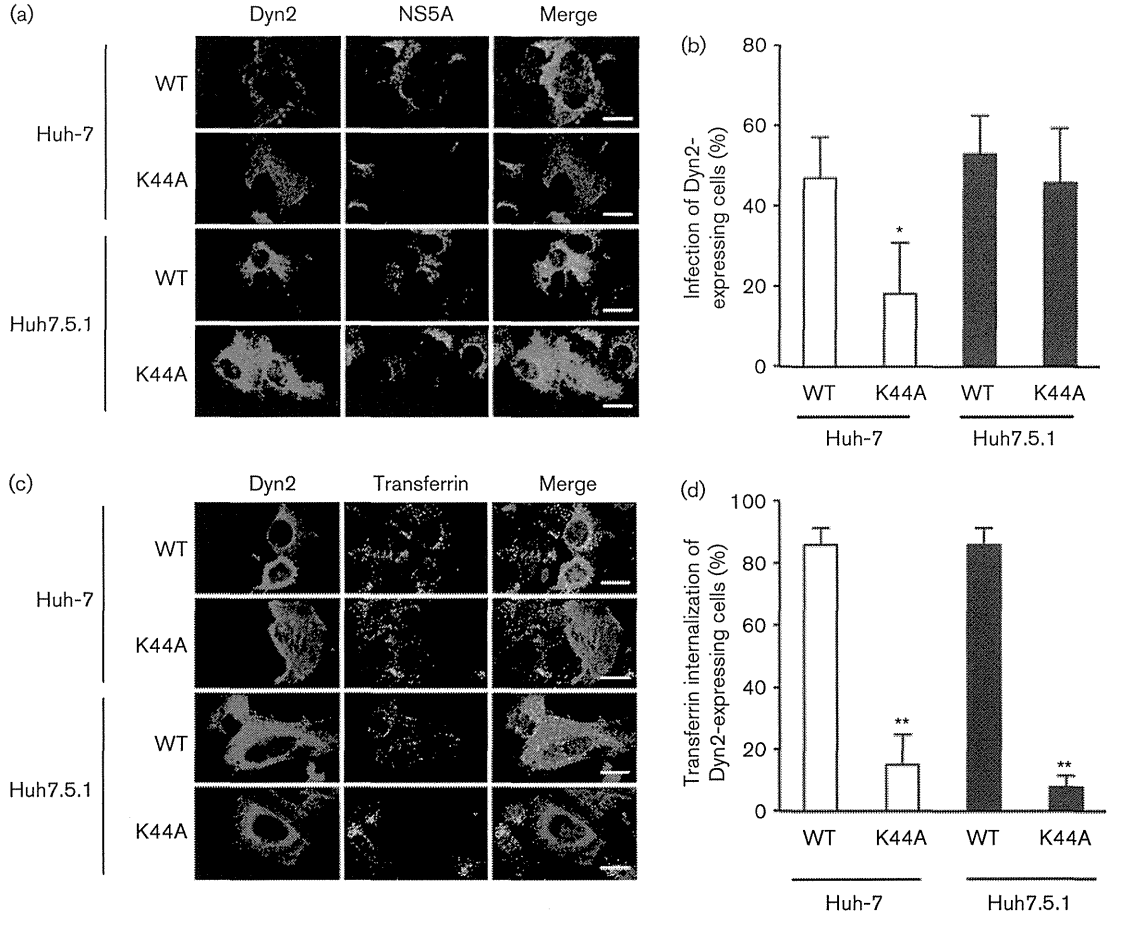

Fig. 4. Dynamin participates in the internalization of HCV in Huh-7 cells, but not in Huh7.5.1 cells. (a) Cells were transfected with HA-tagged WT Dyn2 (Dyn-WT) or dominant-negative Dyn2 (Dyn-K44A) expression plasmids. At 2 days post-transfection, cells were infected with HCVtcp, which possessed a subgenomic replicon without the luciferase gene. After 3 days, cells were fixed and HA-Dyn2 or HCV NS5A stained with anti-HA or anti-NS5A antibodies, respectively. Cell nuclei were counterstained with DAPI. Bar, 100 μm. (b) Data were quantified as the population of HCVtcp-infected cells among HA-positive cells. At least 20 HA-positive cells were evaluated in triplicate experiments. Data represent the mean ± SD. (c) Cells were transfected with HA-tagged Dyn-WT or Dyn-K44A expression plasmids. At 2 days post-transfection, cells were incubated with Alexa Fluor-488 labelled transferrin at 37 °C in a 5% CO_2 incubator. After 30 min of incubation, cells were washed, fixed and stained with anti-HA antibodies. Cell nuclei were counterstained with DAPI. Bar, 100 μm. (d) Data were quantified as the population of transferrin-internalized cells among HA-positive cells. At least 20 HA-positive cells were evaluated in triplicate experiments. Data represent the mean ± SD. Statistical differences between Dyn-WT and Dyn-K44A were evaluated using Student's *t*-test. **P*<0.05, ***P*<0.001 versus Dyn-WT.

including flotillin-dependent endocytosis, ADP-ribosylation factor 6 (Arf6)-dependent endocytosis, clathrin-independent carrier/glycosylphosphatidylinositol-enriched early endosomal compartment (CLIC/GEEC) endocytic pathway and macropinocytosis in Huh7.5.1 cells. Flotillin-1 and Arf6 are indispensable components of the flotillin and Arf6 pathways, respectively. Knockdown of flotillin-1 or Arf6 had no inhibitory effects on HCVtcp infection in Huh7.5.1 cells (Fig. 5a). The CLIC/GEEC endocytic pathway has recently become better defined and is regulated by the GTPase regulator associated with focal adhesion kinase-1 (GRAF1). However, GRAF1 was not detected in Huh-7 or Huh7.5.1 cells (Fig. 5b); thus, it is unlikely that the CLIC/GEEC pathway was involved in HCV entry in Huh7.5.1 cells. In addition, knockdown of p21-activated kinase 1 (PAK1) and the PAK1 effector C-terminal binding protein 1 of E1A (CtBP1), which play important regulatory roles in the process of macropinocytosis, did not inhibit HCVtcp infection in Huh7.5.1 cells (Fig. 5c). Taken together, these results suggested that the entry of HCVtcp into Huh7.5.1 cells was not mediated mainly by flotillin-dependent endocytosis, Arf6-dependent endocytosis, the CLIC/GEEC endocytic pathway and macropinocytosis.

Clathrin-dependent and -independent pathways for HCV entry in other hepatic cells

We further examined the endocytosis pathways for HCV in non-Huh-7-related human liver-derived cell lines. Three HCVcc permissive hepatocellular carcinoma cell lines, Li23-derived ORL8c (Kato *et al.*, 2009), HepCD81/miR122 cells (HepG2/CD81 cells overexpressing miR122) and Hep3B/miR122 (Kambara *et al.*, 2012), were transfected with siRNA for CHC, Dyn2 or claudin-1, followed by infection with HCVtcp. Immunoblotting was performed in order to confirm knockdown of target proteins (Fig. 6a). Although knockdown of CHC or Dyn2 expression inhibited HCVtcp infection of ORL8c and HepCD81/miR122 cells, HCVtcp infection of Hep3B/miR122 cells was not affected (Fig. 6b), thus suggesting that productive entry of HCV is clathrin- and dynamin-independent in Hep3B/miR122 cells.

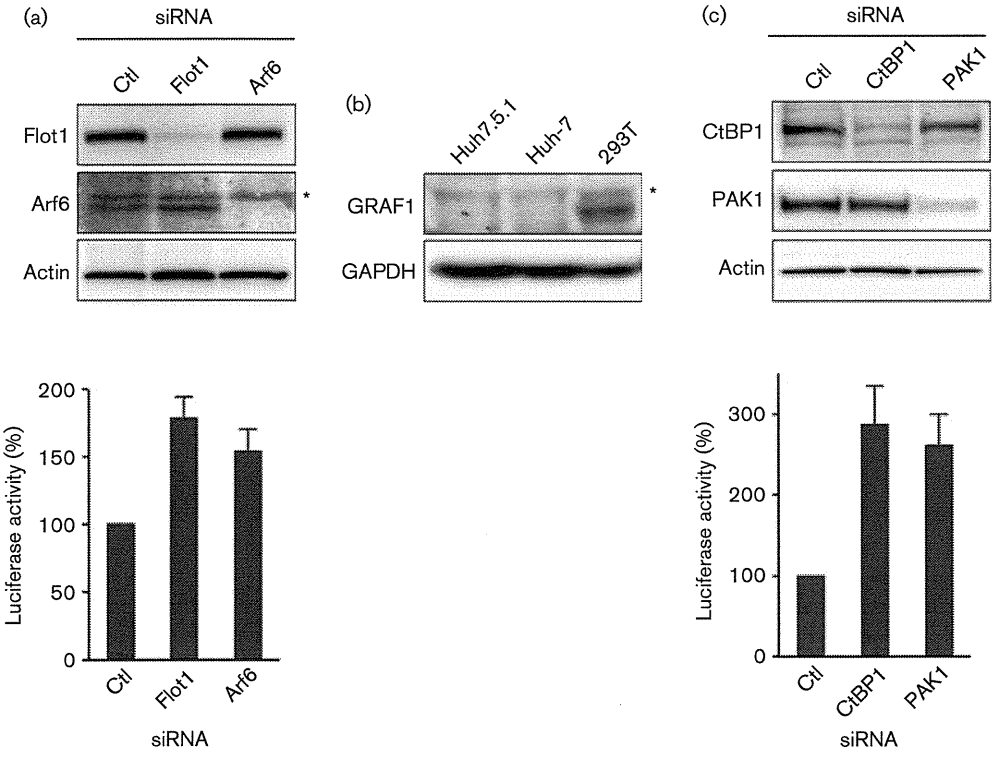

Fig. 5. Role of an alternative endocytosis pathway of HCV in Huh7.5.1 cells. (a) Huh7.5.1 cells were transfected with flotillin-1 (Flot1) or Arf6 siRNAs and specific knockdown of each protein was verified by immunoblotting (upper). Non-specific bands are marked with an asterisk. Cells transfected with siRNA were infected with HCVtcp. Luciferase activity (lower) was determined at 72 h post-infection and expressed relative to the amount observed in control (Ctl) siRNA transfection, Data represent the mean ± SD. (b) Expression of GRAF1 and glyceraldehyde 3-phosphate dehydrogenase (GAPDH) in Huh7.5.1, Huh-7 and 293T cells was analysed by immunoblotting. Non-specific bands are marked with an asterisk. (c) Huh7.5.1 cells were transfected with CtBP1 or PAK1 siRNA and specific knockdown of each protein was verified by immunoblotting (upper). Cells transfected with siRNA were infected with the HCVtcp. Luciferase activity (lower) was determined at 72 h post-infection and expressed relative to the amount observed in control (Ctl) siRNA transfection. Data represent the mean ± SD.

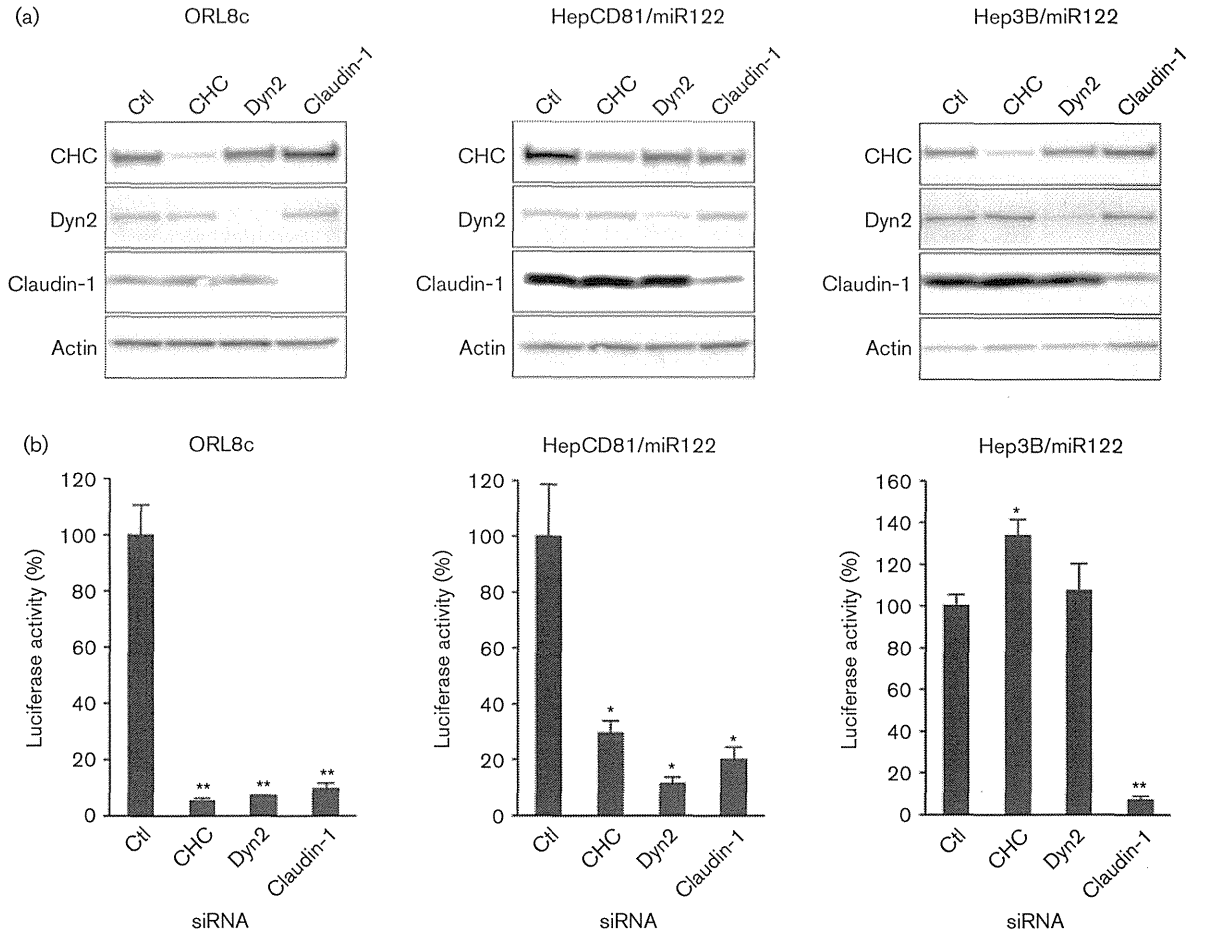

Fig. 6. Clathrin-dependent and -independent pathway of HCV entry in other HCV-permissive cells. The indicated cells were transfected with the indicated siRNAs and then infected with HCVtcp at 48 h post-transfection. (a) Specific knockdown of each protein was verified by immunoblotting. (b) Luciferase activity was determined at 72 h post-infection and expressed relative to the amount observed in the control (Ctl) siRNA transfection. Data represent the mean ± SD. Statistical differences between controls and each siRNA were evaluated using Student's *t*-test. **P*<0.05, ***P*<0.001 versus control.

In summary, we identified an alternative clathrin- and dynamin-independent entry pathway for HCV in at least two independent cell lines, Huh7.5.1 and Hep3B/miR122 cells, in addition to the previously reported clathrin- and dynamin-dependent pathway. These findings provided clues for understanding the molecular mechanisms of the endocytosis pathway for HCV infection.

DISCUSSION

Many viruses have been shown to utilize a number of different endocytic pathways to productively infect their hosts. Clathrin-dependent endocytosis would appear to be the most commonly used, but it is increasingly clear that a number of clathrin-independent endocytosis pathways are also used by several different viruses (Mercer *et al.*, 2010). In the case of HCV, it has been reported that viral entry is mediated by clathrin-dependent endocytosis (Blanchard *et al.*, 2006; Codran *et al.*, 2006; Coller *et al.*, 2009; Meertens *et al.*, 2006; Trotard *et al.*, 2009). In these papers, HCVpp was used at least in part for analysis of HCV entry pathway. However, recent reports have revealed several different characteristics between HCVpp and HCVcc.

Viral entry has been addressed primarily by pharmacologic inhibitor studies, immunofluorescence and electron microscopy, by transfection with dominant-negative constructs, and more recently by siRNA knockdown. Analysis of endocytosis pathways using pharmacological inhibitors has raised concerns about specificity. For example, chlorpromazine, an inhibitor of clathrin-mediated endocytosis, has been shown to exert multiple side-effects on cell function as it targets numerous receptors and intracellular enzymes, and alters plasma membrane characteristics (Sieczkarski & Whittaker, 2002a). Methods for elucidating the viral endocytosis pathway by co-localization of virus particles with host factor also have limitations. Electron and

fluorescence microscopy, which require a high particle number, do not allow the differentiation of infectious and non-infectious particles. Infectious particles of HCV in the supernatant of infected cells appeared to represent only a small portion of secreted virus particles (Akazawa *et al.*, 2008) and it is unclear whether the viral particles observed by microscopy could lead to productive infection. Therefore, we utilized HCVtcp, which is useful for determining productive entry of the virus without reinfection, and a combination of siRNA knockdown and dominant-negative mutants for analysis of the productive route of infection. Although HCVcc is also utilized in analysis of productive entry, it cannot completely exclude the effects of reinfection by virus produced by infected cells. Reduction of HCVcc infection by knockdown of CHC and Dyn2 was moderate when compared with that of HCVtcp (Fig. 3c, d), thus suggesting slight effects due to reinfection in HCVcc.

The data presented here demonstrate for the first time to our knowledge that HCV is able to enter cells via dynamin-independent endocytosis in addition to the previously described classical clathrin- and dynamin-dependent pathway. First, knockdown of CHC and Dyn2 had no inhibitory effects on HCVtcp and HCVcc entry into Huh7.5.1 cells. Second, overexpression of dominant-negative Dyn2 had no inhibitory effects on HCVtcp in Huh7.5.1 cells. Finally, in addition to Huh7.5.1 cells, Hep3B/miR122 cells were also shown to be infected with HCV via clathrin- and dynamin-independent pathways. We further investigated the role of alternative minor routes of HCV entry into Huh7.5.1 cells; however, the productive endocytosis pathway could not be defined. It should be noted that inhibition of alternative endocytosis routes by siRNA led to an increase of luciferase activity (Figs 3c and 5a, c). This could be explained by the inhibition of a particular endocytosis pathway resulting in a compensatory increase in alternative endocytosis pathways (Damke *et al.*, 1995).

Although we confirmed an alternative endocytosis pathway for the productive entry of HCV, it is not clear why and how the two independent endocytosis pathways operate in different cell lines. SV40 can enter cells via caveolae-dependent (Norkin *et al.*, 2002; Pelkmans *et al.*, 2001) and -independent (Damm *et al.*, 2005) pathways. Influenza virus enters cells via clathrin-mediated endocytosis (Matlin *et al.*, 1981) in addition to non-clathrin-mediated, non-caveola-mediated internalization pathways (Sieczkarski & Whittaker, 2002b). Entry of dengue virus type 2 is clathrin-dependent in HeLa and C6/36 cells (Acosta *et al.*, 2008; Mosso *et al.*, 2008; van der Schaar *et al.*, 2008), and is clathrin-independent in Vero cells (Acosta *et al.*, 2009). Different receptor usage may determine the consequential route of entry. However, we did not observe any differences between Huh-7 and Huh7.5.1 cells in terms of knockdown effects of receptor candidate molecules on HCV infection, as shown in Fig. 1(c), although we cannot exclude the possibility that other undefined receptors are associated with viral entry. Huh7.5.1 cells were established by elimination of the HCV genome from replicon cells derived from Huh-7 cells (Blight *et al.*, 2002; Zhong *et al.*, 2005) and they exhibit more potent replication of HCV than the original Huh-7 cells. Further study showed that the increased permissiveness of cured cells results from a mutation in the retinoic acid-inducible gene I (Sumpter *et al.*, 2005), which impairs IFN signalling. In addition, it has been shown that cured cell lines express higher levels of miR122 than parental cells participating in the efficient propagation of HCVcc (Kambara *et al.*, 2012). As it is unclear whether these changes are the reason for a distinct endocytosis pathway, it will be of interest to explore these associations in further studies.

In conclusion, we confirmed an alternative clathrin-independent endocytosis pathway in HCV-permissive human hepatic-derived cells, in addition to the previously reported clathrin-dependent endocytosis pathway. This paper highlights the fact that clathrin- and dynamin-mediated endocytosis is the main route of HCV entry for Huh-7, HepCD81/miR122 and ORL8c cells, whilst clathrin and dynamin do not play a major role during the productive route of HCV infection in Huh7.5.1 and Hep3B/miR122 cells. Taken together, these studies suggest that different cell entry pathways for HCV infection may be utilized in different cell types, although further studies are necessary in order to understand this phenomenon.

METHODS

Cells. The human hepatocellular carcinoma cell lines Huh-7, Huh7.5.1, Hep3B/miR122 and HepG2/CD81, which overexpressed miR122 (Kambara *et al.*, 2012), were maintained in Dulbecco's modified Eagle's medium (DMEM; Wako Pure Chemical Industries) containing non-essential amino acids, penicillin (100 U ml^{-1}), streptomycin (100 $\mu g\ ml^{-1}$) and 10 % FBS. Li23-derived ORL8c cells (Kato *et al.*, 2009) were maintained in F12 medium and DMEM (1 : 1, v/v) supplemented with 1 % FBS, epidermal growth factor (50 ng ml^{-1}), insulin (10 $\mu g\ ml^{-1}$), hydrocortisone (0.36 $\mu g\ ml^{-1}$), transferrin (5 $\mu g\ ml^{-1}$), linoleic acid (5 $\mu g\ ml^{-1}$), selenium (20 ng ml^{-1}), prolactin (10 ng ml^{-1}), gentamicin (10 $\mu g\ ml^{-1}$), kanamycin monosulfate (0.2 mg ml^{-1}) and fungizone (0.5 $\mu g\ ml^{-1}$). All cell lines were cultured at 37 °C in a 5 % CO_2 incubator.

Preparation of viruses. HCVtcp and HCVcc derived from JFH-1 with adaptive mutations in E2 (N417S), p7 (N765D) and NS2 (Q1012R) were generated as described previously (Suzuki *et al.*, 2012). For HepCD81/miR122 and ORL8c cells, HCVtcp containing the *Gaussia* luciferase (GLuc) reporter gene were used. To do this, plasmid pHH/SGR-JFH1/GLuc/NS3m carrying the bicistronic subgenomic HCV replicon containing the GLuc reporter gene and the NS3 adaptive mutation was constructed by replacement of the firefly luciferase (FLuc) gene of pHH/SGR-Luc containing the NS3 mutation (N1586D) (Suzuki *et al.*, 2012) with the GLuc gene of pCMV-GLuc (NEB).

Plasmids. HA-tagged Dyn2, a dominant-negative Dyn2 (K44A) in which Lys44 was replaced with Ala, was cloned into pcDNA3.1 as described previously (Kataoka *et al.*, 2012).

Gene silencing by siRNA. siRNAs were purchased from Sigma-Aldrich and were introduced into the cells at a final concentration of

30 nM using Lipofectamine RNAiMAX (Invitrogen) in accordance with the manufacturer's instructions. Target sequences of the siRNAs were: occludin (5′-GCAAGAUCACUAUGAGACA-3′), SR-BI (5′-GAGCUUUGGCCUUGGUCUA-3′), CD81 (5′-CUGUGAUCAUGAUCUUCGA-3′), CHC (5′-CUAGCUUUGCACAGUUUAA-3′), Dyn2 (5′-CCCUCAAGGAGGCGCUCAA-3′), Cav1 (5′-CCCUAAACACCUCAACGAU-3′), flotillin-1 (5′-CCUAUGACAUCGAGGUCAA-3′), Arf6 (5′-CAGUUCUUGGUAAAGUCCU-3′), CtBP1 (5′-GACUCGACGCUGUGCCACA-3′) and PAK1 (5′-GCAUCAAUUCCUGAAGAUU-3′). Target sequences of the siRNAs for claudin-1, PI4K and scrambled negative control were as described previously (Suzuki *et al.*, 2013).

Immunoblotting. Cells were washed with PBS and incubated with passive lysis buffer (Promega). Lysates were sonicated for 10 min and added to the same volume of 2× SDS-PAGE sample buffer. Protein samples were boiled for 10 min, separated by SDS-PAGE and then transferred to PVDF membranes (Merck Millipore). After blocking, membranes were probed with primary antibodies, followed by incubation with peroxidase-conjugated secondary antibody. Antigen–antibody complexes were visualized using an enhanced chemiluminescence detection system (SuperSignal West Pico Chemiluminescent Substrate; Thermo Scientific) in accordance with the manufacturer's protocols.

Flow cytometry. Cultured cells detached by treatment with trypsin were incubated with anti-CD81 antibody or anti-mouse IgG antibody for 1 h at 4 °C. After being washed with PBS containing 0.1 % BSA, cells were incubated with an Alexa Fluor 488-conjugated anti-mouse secondary antibody (Invitrogen) for 1 h at 4 °C, washed repeatedly and resuspended in PBS. Analyses were performed using a FACSCalibur system (Becton Dickinson).

Reagents and antibodies. Bafilomycin A1 was obtained from Wako Pure Chemical Industries. Alexa Fluor 488-conjugated transferrin was obtained from Invitrogen. For immunoblotting, anti-SR-BI (NB400-104; Novus Biologicals), anti-occludin (71-1500; Invitrogen), anti-claudin-1 (51-9000; Invitrogen), anti-Dyn2 (ab3457; Abcam), anti-Cav1 (N-20; Santa Cruz Biotechnology), anti-flotillin (H-104; Santa Cruz Biotechnology), anti-Arf6 (ab77581; Abcam) and anti-PAK1 (2602; Cell Signaling Technology) rabbit polyclonal antibodies; anti-CD81 (JS-81; BD Biosciences), anti-β-actin (AC-15; Sigma-Aldrich), anti-CHC (23; BD Biosciences), anti-GRAF1 (SAB1400439; Sigma-Aldrich) and anti-glyceraldehyde 3-phosphate dehydrogenase (6C5; Merck Millipore) mouse mAb; and anti-CtBP1 goat polyclonal antibody (C-17; Santa Cruz Biotechnology) were used. For immunofluorescence staining, anti-CHC mAb (X22) and anti-HA rat polyclonal antibody (3F10) were obtained from Thermo Scientific and Roche Applied Science, respectively. Anti-NS5A antibody was a rabbit polyclonal antibody against synthetic peptides. Alexa Fluor 488- or 555-labelled secondary antibodies were obtained from Invitrogen.

DNA transfection. Cell monolayers were transfected with plasmid DNA using TransIT-LT1 transfection reagent (Mirus) in accordance with the manufacturer's instructions.

Treatment of cells with bafilomycin A1 and cell viability. Cells were preincubated with various concentrations of bafilomycin A1 for 60 min at 37 °C. Preincubated cells were then infected with HCVtcp. Cells treated with 0.1 % DMSO were used as controls. Cell viability was analysed by the Cell Titre-Glo Luminescent Cell Viability Assay (Promega).

Uptake of transferrin. Cells were grown on glass coverslips. After cells were transfected with HA-tagged Dyn2 expression plasmids, Alexa Fluor 488-conjugated transferrin at 20 μg ml^{-1} was added and incubated for 30 min. Cells were washed with PBS and fixed in 4 % paraformaldehyde.

Immunofluorescence analysis. Huh7.5.1 and Huh-7 cells were fixed with 4 % paraformaldehyde in PBS for 30 min, and were then blocked and permeabilized with 0.3 % Triton X-100 in a non-fat milk solution (Block Ace; Snow Brand Milk Products) for 60 min at room temperature. Samples were then incubated with anti-CHC, anti-Dyn2, anti-Cav1, anti-NS5A or anti-HA for 60 min at room temperature, washed three times with PBS, and then incubated with secondary antibodies for 60 min at room temperature. Finally, samples were washed three times with PBS, rinsed briefly in double-distilled H_2O and mounted with DAPI mounting medium. The signal was analysed using a Leica TCS SPE confocal microscope.

Luciferase assay. For quantification of FLuc activity in HCVtcp-infected cells, cells were lysed with passive lysis buffer (Promega) at 72 h post-infection. FLuc activity of the cells was determined using a luciferase assay system (Promega). For quantification of GLuc activity in supernatants of HCVtcp-infected cells, the *Renilla* Luciferase Assay System (Promega) was used. All luciferase assays were performed at least in triplicate.

Quantification of HCV core protein. HCV core protein was quantified using a highly sensitive enzyme immunoassay (Lumipulse G1200; Fujirebio) in accordance with the manufacturer's instructions.

ACKNOWLEDGEMENTS

We are grateful to Francis V. Chisari (Scripps Research Institute) for providing Huh-7 and Huh7.5.1 cells. We would also like to thank M. Sasaki for technical assistance, and T. Kato, A. Murayama and K. Mori for helpful discussion.

REFERENCES

Acosta, E. G., Castilla, V. & Damonte, E. B. (2008). Functional entry of dengue virus into *Aedes albopictus* mosquito cells is dependent on clathrin-mediated endocytosis. *J Gen Virol* **89**, 474–484.

Acosta, E. G., Castilla, V. & Damonte, E. B. (2009). Alternative infectious entry pathways for dengue virus serotypes into mammalian cells. *Cell Microbiol* **11**, 1533–1549.

Akazawa, D., Date, T., Morikawa, K., Murayama, A., Omi, N., Takahashi, H., Nakamura, N., Ishii, K., Suzuki, T. & other authors (2008). Characterization of infectious hepatitis C virus from liver-derived cell lines. *Biochem Biophys Res Commun* **377**, 747–751.

Bartosch, B., Vitelli, A., Granier, C., Goujon, C., Dubuisson, J., Pascale, S., Scarselli, E., Cortese, R., Nicosia, A. & Cosset, F. L. (2003). Cell entry of hepatitis C virus requires a set of co-receptors that include the CD81 tetraspanin and the SR-B1 scavenger receptor. *J Bio Chem* **278**, 41624–41630.

Benedicto, I., Molina-Jimenez, F., Bartosch, B., Cosset, F. L., Lavillette, D., Prieto, J., Moreno-Otero, R., Valenzuela-Fernandez, A., Aldabe, R., Lopez-Cabrera, M. & Majano, P. L. (2009). The tight junction-associated protein occludin is required for a postbinding step in hepatitis C virus entry and infection. *J Virol* **83**, 8012–8020.

Blanchard, E., Belouzard, S., Goueslain, L., Wakita, T., Dubuisson, J., Wychowski, C. & Rouillé, Y. (2006). Hepatitis C virus entry depends on clathrin-mediated endocytosis. *J Virol* **80**, 6964–6972.

Blight, K. J., McKeating, J. A. & Rice, C. M. (2002). Highly permissive cell lines for subgenomic and genomic hepatitis C virus RNA replication. *J Virol* **76**, 13001–13014.

Codran, A., Royer, C., Jaeck, D., Bastien-Valle, M., Baumert, T. F., Kieny, M. P., Pereira, C. A. & Martin, J. P. (2006). Entry of hepatitis C

virus pseudotypes into primary human hepatocytes by clathrin-dependent endocytosis. *J Gen Virol* **87**, 2583–2593.

Coller, K. E., Berger, K. L., Heaton, N. S., Cooper, J. D., Yoon, R. & Randall, G. (2009). RNA interference and single particle tracking analysis of hepatitis C virus endocytosis. *PLoS Pathog* **5**, e1000702.

Damke, H., Baba, T., van der Bliek, A. M. & Schmid, S. L. (1995). Clathrin-independent pinocytosis is induced in cells overexpressing a temperature-sensitive mutant of dynamin. *J Cell Biol* **131**, 69–80.

Damm, E. M., Pelkmans, L., Kartenbeck, J., Mezzacasa, A., Kurzchalia, T. & Helenius, A. (2005). Clathrin- and caveolin-1-independent endocytosis: entry of simian virus 40 into cells devoid of caveolae. *J Cell Biol* **168**, 477–488.

Evans, M. J., von Hahn, T., Tscherne, D. M., Syder, A. J., Panis, M., Wolk, B., Hatziioannou, T., McKeating, J. A., Bieniasz, P. D. & Rice, C. M. (2007). Claudin-1 is a hepatitis C virus co-receptor required for a late step in entry. *Nature* **446**, 801–805.

Grove, J. & Marsh, M. (2011). The cell biology of receptor-mediated virus entry. *J Cell Biol* **195**, 1071–1082.

Grove, J., Nielsen, S., Zhong, J., Bassendine, M. F., Drummer, H. E., Balfe, P. & McKeating, J. A. (2008). Identification of a residue in hepatitis C virus E2 glycoprotein that determines scavenger receptor BI and CD81 receptor dependency and sensitivity to neutralizing antibodies. *J Virol* **82**, 12020–12029.

Helle, F., Vieyres, G., Elkrief, L., Popescu, C.-I., Wychowski, C., Descamps, V., Castelain, S., Roingeard, P., Duverlie, G. & Dubuisson, J. (2010). Role of N-linked glycans in the functions of hepatitis C virus envelope proteins incorporated into infectious virions. *J Virol* **84**, 11905–11915.

Hoofnagle, J. H. (2002). Course and outcome of hepatitis C. *Hepatology* **36** (Suppl 1), S21–S29.

Kambara, H., Fukuhara, T., Shiokawa, M., Ono, C., Ohara, Y., Kamitani, W. & Matsuura, Y. (2012). Establishment of a novel permissive cell line for the propagation of hepatitis C virus by expression of microRNA miR122. *J Virol* **86**, 1382–1393.

Kataoka, C., Kaname, Y., Taguwa, S., Abe, T., Fukuhara, T., Tani, H., Moriishi, K. & Matsuura, Y. (2012). Baculovirus GP64-mediated entry into mammalian cells. *J Virol* **86**, 2610–2620.

Kato, N., Mori, K., Abe, K., Dansako, H., Kuroki, M., Ariumi, Y., Wakita, T. & Ikeda, M. (2009). Efficient replication systems for hepatitis C virus using a new human hepatoma cell line. *Virus Res* **146**, 41–50.

Liu, S., Yang, W., Shen, L., Turner, J. R., Coyne, C. B. & Wang, T. (2009). Tight junction proteins claudin-1 and occludin control hepatitis C virus entry and are downregulated during infection to prevent superinfection. *J Virol* **83**, 2011–2014.

Lupberger, J., Zeisel, M. B., Xiao, F., Thumann, C., Fofana, I., Zona, L., Davis, C., Mee, C. J., Turek, M. & other authors (2011). EGFR and EphA2 are host factors for hepatitis C virus entry and possible targets for antiviral therapy. *Nat Med* **17**, 589–595.

Marsh, M. & Helenius, A. (2006). Virus entry: open sesame. *Cell* **124**, 729–740.

Matlin, K. S., Reggio, H., Helenius, A. & Simons, K. (1981). Infectious entry pathway of influenza virus in a canine kidney cell line. *J Cell Biol* **91**, 601–613.

McKeating, J. A., Zhang, L. Q., Logvinoff, C., Flint, M., Zhang, J., Yu, J., Butera, D., Ho, D. D., Dustin, L. B., Rice, C. M. & Balfe, P. (2004). Diverse hepatitis C virus glycoproteins mediate viral infection in a CD81-dependent manner. *Journal of virology* **78**, 8496–8505.

Meertens, L., Bertaux, C. & Dragic, T. (2006). Hepatitis C virus entry requires a critical postinternalization step and delivery to early endosomes via clathrin-coated vesicles. *J Virol* **80**, 11571–11578.

Mercer, J., Schelhaas, M. & Helenius, A. (2010). Virus entry by endocytosis. *Annu Rev Biochem* **79**, 803–833.

Miaczynska, M. & Stenmark, H. (2008). Mechanisms and functions of endocytosis. *J Cell Biol* **180**, 7–11.

Mosso, C., Galván-Mendoza, I. J., Ludert, J. E. & del Angel, R. M. (2008). Endocytic pathway followed by dengue virus to infect the mosquito cell line C6/36 HT. *Virology* **378**, 193–199.

Norkin, L. C., Anderson, H. A., Wolfrom, S. A. & Oppenheim, A. (2002). Caveolar endocytosis of simian virus 40 is followed by brefeldin A-sensitive transport to the endoplasmic reticulum, where the virus disassembles. *J Virol* **76**, 5156–5166.

Pelkmans, L., Kartenbeck, J. & Helenius, A. (2001). Caveolar endocytosis of simian virus 40 reveals a new two-step vesicular-transport pathway to the ER. *Nat Cell Biol* **3**, 473–483.

Pileri, P., Uematsu, Y., Campagnoli, S., Galli, G., Falugi, F., Petracca, R., Weiner, A. J., Houghton, M., Rosa, D., Grandi, G. & Abrignani, S. (1998). Binding of hepatitis C virus to CD81. *Science* **282**, 938–941.

Ploss, A., Evans, M. J., Gaysinskaya, V. A., Panis, M., You, H., de Jong, Y. P. & Rice, C. M. (2009). Human occludin is a hepatitis C virus entry factor required for infection of mouse cells. *Nature* **457**, 882–886.

Sainz, B., Jr, Barretto, N., Martin, D. N., Hiraga, N., Imamura, M., Hussain, S., Marsh, K. A., Yu, X., Chayama, K. & other authors (2012). Identification of the Niemann–Pick C1-like 1 cholesterol absorption receptor as a new hepatitis C virus entry factor. *Nat Med* **18**, 281–285.

Scarselli, E., Ansuini, H., Cerino, R., Roccasecca, R. M., Acali, S., Filocamo, G., Traboni, C., Nicosia, A., Cortese, R. & Vitelli, A. (2002). The human scavenger receptor class B type I is a novel candidate receptor for the hepatitis C virus. *Embo J* **21**, 5017–5025.

Sieczkarski, S. B. & Whittaker, G. R. (2002a). Dissecting virus entry via endocytosis. *J Gen Virol* **83**, 1535–1545.

Sieczkarski, S. B. & Whittaker, G. R. (2002b). Influenza virus can enter and infect cells in the absence of clathrin-mediated endocytosis. *J Virol* **76**, 10455–10464.

Sumpter, R., Jr, Loo, Y.-M., Foy, E., Li, K., Yoneyama, M., Fujita, T., Lemon, S. M. & Gale, M., Jr (2005). Regulating intracellular antiviral defense and permissiveness to hepatitis C virus RNA replication through a cellular RNA helicase, RIG-I. *J Virol* **79**, 2689–2699.

Suzuki, T., Ishii, K., Aizaki, H. & Wakita, T. (2007). Hepatitis C viral life cycle. *Adv Drug Deliv Rev* **59**, 1200–1212.

Suzuki, R., Saito, K., Kato, T., Shirakura, M., Akazawa, D., Ishii, K., Aizaki, H., Kanegae, Y., Matsuura, Y. & other authors (2012). Trans-complemented hepatitis C virus particles as a versatile tool for study of virus assembly and infection. *Virology* **432**, 29–38.

Suzuki, R., Matsuda, M., Watashi, K., Aizaki, H., Matsuura, Y., Wakita, T. & Suzuki, T. (2013). Signal peptidase complex subunit 1 participates in the assembly of hepatitis C virus through an interaction with E2 and NS2. *PLoS Pathog* **9**, e1003589.

Trotard, M., Lepère-Douard, C., Régeard, M., Piquet-Pellorce, C., Lavillette, D., Cosset, F. L., Gripon, P. & Le Seyec, J. (2009). Kinases required in hepatitis C virus entry and replication highlighted by small interference RNA screening. *FASEB J* **23**, 3780–3789.

van der Schaar, H. M., Rust, M. J., Chen, C., van der Ende-Metselaar, H., Wilschut, J., Zhuang, X. & Smit, J. M. (2008). Dissecting the cell entry pathway of dengue virus by single-particle tracking in living cells. *PLoS Pathog* **4**, e1000244.

Vieyres, G., Thomas, X., Descamps, V., Duverlie, G., Patel, A. H. & Dubuisson, J. (2010). Characterization of the envelope glycoproteins associated with infectious hepatitis C virus. *J Virol* **84**, 10159–10168.

Zhong, J., Gastaminza, P., Cheng, G., Kapadia, S., Kato, T., Burton, D. R., Wieland, S. F., Uprichard, S. L., Wakita, T. & Chisari, F. V. (2005). Robust hepatitis C virus infection *in vitro*. *Proc Natl Acad Sci U S A* **102**, 9294–9299.

nature COMMUNICATIONS

ARTICLE

Received 7 Nov 2014 | Accepted 13 Jan 2015 | Published 18 Feb 2015

DOI: 10.1038/ncomms7280

Defined TLR3-specific adjuvant that induces NK and CTL activation without significant cytokine production *in vivo*

Misako Matsumoto[1], Megumi Tatematsu[1], Fumiko Nishikawa[1], Masahiro Azuma[1,†], Noriko Ishii[1], Akiko Morii-Sakai[1], Hiroaki Shime[1] & Tsukasa Seya[1]

Ligand stimulation of the Toll-like receptors (TLRs) triggers innate immune response, cytokine production and cellular immune activation in dendritic cells. However, most TLR ligands are microbial constituents, which cause inflammation and toxicity. Toxic response could be reduced for secure immunotherapy through the use of chemically synthesized ligands with defined functions. Here we create an RNA ligand for TLR3 with no ability to activate the RIG-I/MDA5 pathway. This TLR3 ligand is a chimeric molecule consisting of phosphorothioate ODN-guided dsRNA (sODN-dsRNA), which elicits far less cytokine production than poly(I:C) *in vitro* and *in vivo*. The activation of TLR3/TICAM-1 pathway by sODN-dsRNA effectively induces natural killer and cytotoxic T cells in tumour-loaded mice, thereby establishing antitumour immunity. Systemic cytokinemia does not occur following subcutaneous or even intraperitoneal administration of sODN-dsRNA, indicating that TICAM-1 signalling with minute local cytokines sufficiently activate dendritic cells to prime tumoricidal effectors *in vivo*.

[1] Department of Microbiology and Immunology, Hokkaido University Graduate School of Medicine, Kita 15, Nishi 7, Kita-ku, Sapporo 060-8638, Japan. † Present address: Department of Pathology and Cellular Biology, University of Montreal, 2900 Edouard-Montpetit, Montreal, Quebec, Canada H3T 1J4. Correspondence and requests for materials should be addressed to M.M. (email: matumoto@pop.med.hokudai.ac.jp) or to T.S. (email: seya-tu@pop.med.hokudai.ac.jp).

Double-stranded (ds) RNA is often a signature of viral infection, which induces production of type I interferon (IFN) and inflammatory cytokines[1,2]. Its putative analogue polyinosinic:polycytidylic acid (poly(I:C)) exhibits both strong antiviral and anticancer potential[3,4]. Poly(I:C) has been considered a promising adjuvant for cancer immunotherapy for several decades[4–6]. In mouse models, growth retardation of syngenic implant tumours is observed following administration of poly(I:C)[7,8], which is due to dendritic cell (DC)-derived natural killer (NK) and cytotoxic T-cell (CTL) activity[9,10]. Nevertheless, it has not been successfully used therapeutically in patients with cancer[5,6]. The amount of poly(I:C) required for an adequate therapeutic response causes side effects, including arthlargia, fever, erythema and sometimes life-threatening endotoxin-like shock[5,6], which have prevented application of this dsRNA analogue from the clinical use. These side effects may be related to cytokine storm induced by dsRNA, although the situation is somewhat alleviated when minimal poly(I:C)-LC (poly-L-lysine and methylcellulose) is used instead of effector-inducible doses of mere poly(I:C) alone[5,6,11].

According to recent understanding on pattern recognition of innate immunity, poly(I:C) is a ligand for multiple pattern recognition receptors (PRRs), including protein kinase R, retinoic acid-inducible gene-I (RIG-I), melanoma differentiation-associated gene 5 (MDA5) and Toll-like receptor (TLR) 3 (refs 1,4,12). Virus replication usually produces dsRNA within the cytoplasm of infected cells and stimulates the cytoplasmic RNA sensors[12,13]. In contrast, TLR3 is activated when dsRNA liberated from virus-infected cells is internalized into the endosome of non-infected phagocytes[4,14], such as DCs and macrophages. Type I IFN and DC-mediated immune responses are evoked to suppress virus replication. Physiologically, these responses occur in a complex manner, therefore, what happens *in vivo* when only a single receptor is stimulated remains to be elucidated, whereas what happens *in vivo* when a single gene is disrupted has been reported in knockout (KO) mouse studies[1]. It is therefore crucial in drug design to create PRR ligands specific for each PRR for the development of immune adjuvant.

Regression of tumour with a lesser major histocompatibility complex expression[15] is caused by reciprocal activation of NK cells by poly(I:C)-stimulated DC[9,16]. However, in antitumour immunity, constitutive proliferation of antitumour CTL is important and antigen (Ag)-presenting DC must capture not only innate patterns but also tumour-associated Ag (TAA) for their cross-priming[10,17]. $CD8\alpha^+$ DC in mouse lymphoid tissue[10,18,19] and $CD103^+$ and $CD141^+$ DCs in humans[18–20] are representative subsets that express TLR3 and induce efficient Ag cross-presentation in response to dsRNA enabling presentation of Ags to $CD8^+$ T cells on their major histocompatibility complex class I proteins. In contrast, interleukin (IL)-12, IL-6, tumour necrosis factor (TNF)-α and IFN-α/β are the main mediators released in the serum secondary to exogenously administered poly(I:C)[4,20,21]. Studies in KO mice suggested that TLR3 has a pivotal role in inducing cross-presentation[10,17], but its role is marginal in systemic cytokine/IFN production *in vivo*[21]. Most cytokines (except IL-12 p40) and type I IFN detected in serum are attributable to poly(I:C)'s stimulation of RIG-I and/or MDA5, that is, the mitochondrial antiviral-signalling protein (MAVS) pathway[12,21]. CTL/NK cell activation and robust cytokine production can be assigned, although partly overlapping, to the TLR3/Toll-IL-1 receptor domain-containing adaptor molecule (TICAM)-1 or MAVS pathway, respectively.

Here we generated synthetic dsRNA derivatives expected to specifically act on TLR3, but not on RIG-I/MDA5. These ligands exhibited strong activity in inducing antitumour CTL and NK cells and caused marked regression of tumours without off-target effects including significant increases of serum cytokine/IFN levels in mouse models.

Results

Design of novel TLR3 agonist. What we experienced in developing an RNA adjuvant was that: very little *in vitro* transcribed dsRNAs entered the human cells[22], whereas poly(I:C) as well as CpG or control GpC phosphorothioate oligodeoxynucleotides (sODNs) reached the endosome in human myeloid DCs and epithelial cells. Poly(I:C) and sODNs appeared to share the uptake receptor[23]. To deliver dsRNA to endosome TLR3, we have connected sODN to 5′ sense RNA and annealed it with antisense RNA (Fig. 1a) to guide dsRNA internalization into TLR3-positive endosomes. The RNA source was chosen from a vaccine strain of measles virus (MV), as children around the world undergo MV vaccination without severe adverse events. Because >40 bp dsRNA may be the minimal length for activation of TLR3 (ref. 24), we selected the region of defective interference RNA in the vaccine MV that causes no RNA interference[25].

Because direct chemical synthesis of long sequences of RNA was unfeasible in our laboratory until recently, we first made the RNA duplex structures by *in vitro* transcription and annealing. sODN was connected via a linker DNA to dsRNA, so the three-chain structures were first designed (Fig. 1b) to carry forward by many trial-and-error tests for a specific TLR3 agonist. A GpC-type sODN cap cM362 (Fig. 1a,b) facilitates targeting to TLR3-positive endosomes, does not activate TLR9 and blocks dsRNA-mediated RIG-I/MDA5 activation; therefore it meets our criteria for a single PRR agonist.

Testing function of *in vitro* transcribed sODN-dsRNAs. Various kinds of sODN-dsRNA hybrid molecules were prepared by *in vitro* transcription and annealing (Supplementary Fig. 1a, Supplementary Tables 1 and 2). In preliminary experiments to screen for a preferential sODN-dsRNA, we tested reporter gene (Luc125 for IFN-β promoter) activation in HEK293 cells expressing human TLR3.

sODN-dsRNAs with dsRNA of >99 bp in length induced TLR3-dependent IFN-β-promoter activation similar to that induced by poly(I:C) in the presence or absence of fetal calf serum (FCS), whereas sODN-dsRNAs with dsRNA of <79 bp induced hardly any activation of TLR3 (Supplementary Fig. 1b,c). Notably, none of the sODN-dsRNAs examined were able to activate cytoplasmic RNA sensors when transfected into HEK293 cells (Supplementary Fig. 2). We examined whether GpC motif or the length of sODN influenced the uptake of sODN-dsRNA. TLR3-mediated IFN-β promoter activation by sODN-dsRNA was independent of the presence of a GpC motif of sODN but dependent on the length; almost >20-mer of sODN is required for full activation of endosomal TLR3 (Supplementary Fig. 3). 139 bp dsRNA and control B-type (c2006) or C-type (cM362) sODN were good candidates for activation of endosomal TLR3 with no TLR9 activation.

We next examined the internalization of Cy3-labelled cM362-dsRNA (cM362-79, cM362-99 and cM362-139) in HeLa cells. cM362-dsRNAs were all similarly bound to the cell surface at 4 °C, but dsRNA73 and dsRNA139 without cM362 could not bind (Supplementary Fig. 4). When cells were incubated at 37 °C, cM362-99 and cM362-139 both entered the cells more quickly than cM362 and cM362-79, localized in the early endosome after 15 min incubation and were retained for up to 120 min, whereas cM362 and cM362-79 co-localized with EEA1 at a later time point (30 min) and quickly moved to the lysosomes. Localization of cM362-139 in the lysosomes was observed after 60 min

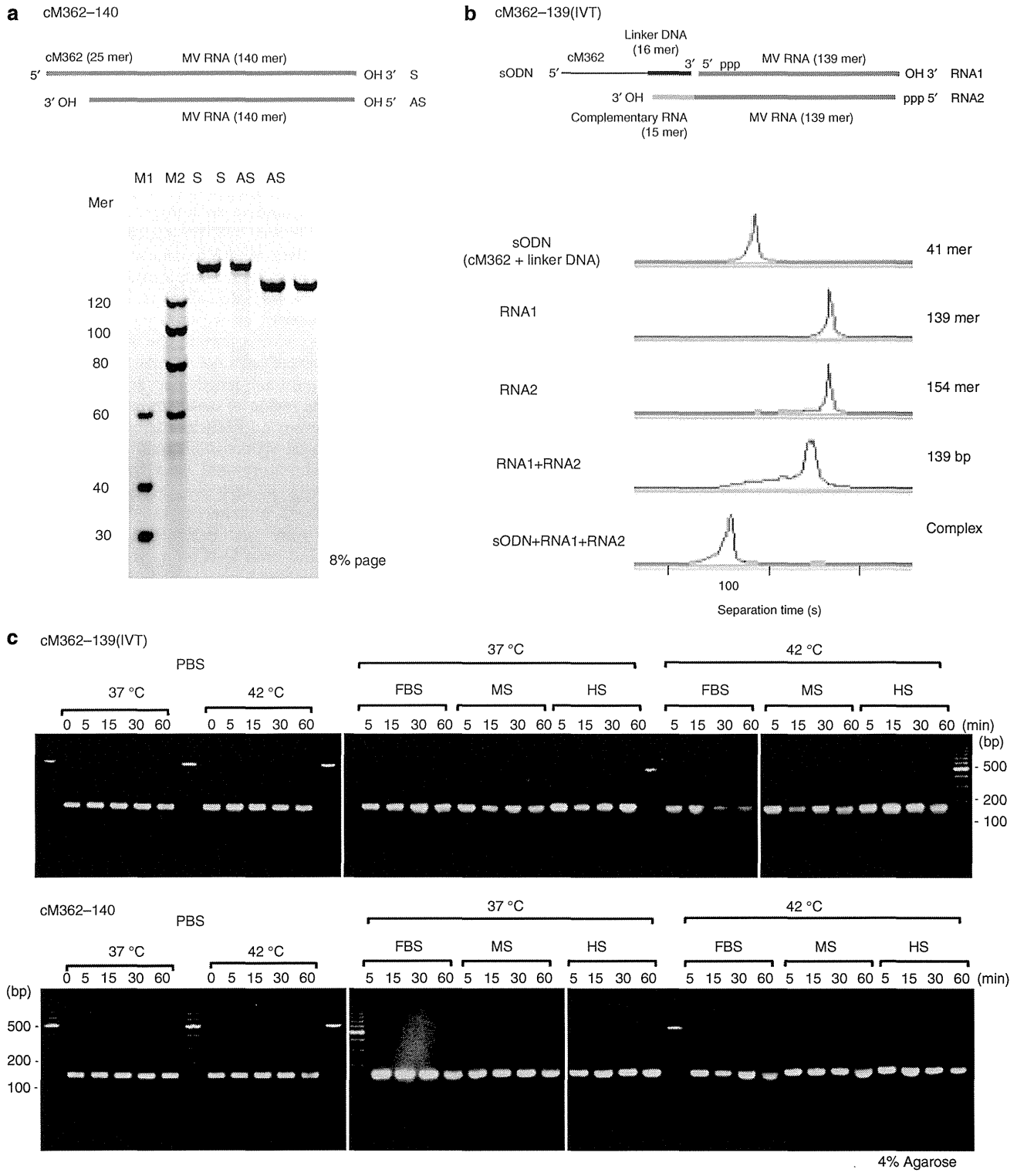

Figure 1 | Preparation of cM362-139 and cM362-140. (**a**) Schematic diagram of cM362-140. cM362-140 consists of chemically synthesized two nucleotide strands. The sense strand (S) is a 140 mer RNA capped with cM362 (25 mer) at 5′ site. The antisense strand (AS) is the complementary 140 mer RNA. Five pmol of S and AS RNAs were analysed on 8% PAGE containing 7M urea. M1 and M2, RNA size markers. (**b**) Schematic diagram of cM362-139(IVT) and its electropherograms. cM362-139(IVT) consists of three nucleotide strands, sODN (cM362 + linker DNA; 41 mer), *in vitro* transcribed sense RNA strand (RNA1; 139 mer) and antisense RNA strand (RNA2; 154 mer). All sequences of DNA and RNAs are described in Supplementary Tables. sODN, RNA1, RNA2, dsRNA (RNA1 + RNA2) and complex cM362-139 (sODN + RNA1 + RNA2) were analysed using multi-channel microchip electrophoresis. (**c**) Stability of cM362-139(IVT) and cM362-140. cM362-139(IVT) and cM362-140 were incubated in PBS with or without 10% heat-inactivated FBS, mouse serum (MS) or human serum (HS) at 37 °C or 42 °C for indicated time points. Aliquots containing 0.1 μg of treated cM362-dsRNAs were loaded onto a 4% agarose gel.

incubation, which was relatively slow compared with cM362-99 (Supplementary Fig. 4). These results suggested that the length of dsRNA together with the presence of cM362 influences the internalization speed and retention time in the TLR3-situated early endosome.

The abilities of cM362-dsRNAs to induce cytokine production were then examined using splenic DCs from wild-type and TLR3-deficient mice. cM362-79 and -139 induced a slight increase in TNF-α and IL-6 production by splenic CD11c$^+$ DCs in a TLR3-dependent manner (Supplementary Fig. 5a). Again, cM362-dsRNAs did not activate cytoplasmic RNA sensors in mouse splenic CD11c$^+$ DCs (Supplementary Fig. 5b). Thus, the chimeric compound cM362-139 appears to possess novel features that enable it to be quickly delivered to TLR3-positive endosomes, retained for a long period in the endosomes, and activate TLR3 but not RIG-like receptor (RLR).

As a TLR3-specific agonist with high activity, we selected cM362-139 for further *in vivo* studies with tumour-loaded mice.

Chemical synthesis of cM362-140. As chemical synthesis of sODN-dsRNA is indispensable for complying with good manufacturing practice (GMP) criteria, we started trials for chemical synthesis of cM362-140 (Fig. 1a), and its activity was analysed in comparison with *in vitro* transcribed cM362-139 (Fig. 1a,b). A synthesized 165 mer sense cM362-RNA hybrid and a 140mer antisense RNA, both of which consisted of single bands on 8% polyacrylamide gel electrophoresis (PAGE) and high-performance liquid chromatography/mass spectrometry analysis were annealed to make cM362-140 (Fig. 1a, lower panel). First, the degradability of cM362-139(IVT) and chemically synthesized cM362-140 were tested under different conditions. Both compounds were stable during incubation in PBS with or without 10% FBS, mouse serum or human serum at 37 °C for 60 min. cM362-139(IVT) was slightly degraded in PBS containing FBS or mouse serum but not human serum during incubation at 42 °C (Fig. 1c). Notably, cM362-139(IVT) was susceptible to degradation by nucleases during incubation in RNase-free water containing 10% FBS or mouse serum, but relatively resistant to human serum (Supplementary Fig. 6). In contrast, cM362-140 was quite stable under all these conditions. Thus, synthetic cM362-140 consisting of the cM362-capped RNA strand and antisense RNA strand was found to be more resistant to serum nucleases than cM362-139(IVT) consisting of three nucleotide strands.

cM362-140 activates TLR3 but not cytoplasmic RNA sensors. cM362-140 efficiently induced TLR3-dependent IFN-β promoter activation similar to cM362-139(IVT), when it was used to stimulate HEK293 cells expressing human TLR3 by simple addition or endosomal delivery (Fig. 2a, left and centre panels). Activation of cytoplasmic RNA/DNA sensors by cM362-140 was hardly observed in HEK293 cells similar to cM362-139(IVT) (Fig. 2a, right panel). To address the potential of cM362-140 for cytokine induction, splenic DCs from wild-type, *Tlr3*$^{-/-}$ or *Mavs*$^{-/-}$ mice were stimulated with poly(I:C), cM362-139(IVT), control synthetic dsRNA140 or cM362-140, either alone or complexed with N-(1-(2,3-Dioleoyloxy)propyl)-N, N, N-trimethylammonium methyl-sulfate) (DOTAP) to deliver them to endosomes, or complexed with Lipofectamine to deliver them to cytoplasm. Extracellular addition of cM362-139(IVT) and cM362-140 to splenic DCs induced a subtle increase in TNF-α, IL-6 and IFN-β production compared with poly(I:C) treatment, whereas synthetic dsRNA140 (with no GpC) did not induce any cytokine over the detection limits (Fig. 2b, left panels). Endosomal delivery of cM362-139(IVT) or cM362-140 with DOTAP also induced minimal levels of TNF-α, IL-6 and IFN-β dependent upon TLR3 (Fig. 2b, centre panels). When the compounds were transfected into cytoplasm with Lipofectamine, MAVS-dependent cytokine production was barely observed with cM362-140, whereas only low levels of IL-6 and IFN-β were induced with cM362-139 in TLR3 KO DC (Fig. 2b, right panel). This MAVS activity may reflect the exposure of a few 5′-triphosphated species of cM362-139(IVT) due to minor RNA degradation. These results indicate that cM362-140 targets endosomal TLR3 and activate the TICAM-1 pathway in both human and mouse cells.

***In vivo* cytokine induction by cM362-140.** Injection of poly(I:C) into mouse peritoneal cavity strongly induced proinflammatory cytokine production in a TLR3-independent manner and high level of TNF-α and IL-6 were detected in sera at 3 h after injection (Fig. 3a). In contrast, both cM362-140 and cM362-139(IVT) hardly induced cytokine production and serum TNF-α, IL-6 and IL-10 levels were very low, which is mediated by TLR3 (Fig. 3a). Unlike poly(I:C), cM362-140 or -139(IVT) induced undetectable levels of IFN-β in wild-type mouse sera (Supplementary Fig. 7).

A subcutaneous (s.c.) injection of cM362-140 induced the mRNAs of IFN-β and IL-6, but not TNF-α, in the inguinal and axillary lymph nodes (LNs) and spleen; the expression level was lower than that induced by poly(I:C) (Fig. 3b). These results suggest that TLR3-specific activation with cM362-140 results in low levels of cytokine production *in vivo* either by intraperitoneal (i.p.) or s.c. administration.

EG7 tumour regression by CTL induced by cM362-139/140. The next question was whether cM362-139(IVT) causes tumour growth retardation as observed with poly(I:C). EG7 cells (a lymphoma cell line containing ovalbumin, OVA) were inoculated into the back of wild-type (WT) C57BL/6 mice, and the indicated materials were injected s.c. around the EG7 tumour that developed (Fig. 4). Tumour growth was mildly retarded by treatment with poly(I:C) or cM362-139(IVT) alone (Fig. 4a). Combination therapy of OVA and poly(I:C) or cM362-139(IVT) resulted in complete remission of EG7 tumour >12 days after the treatment (Fig. 4a). The results infer that the combination of RNA adjuvant + tumour Ag exerts antitumour immune effect in spite of the low induction of proinflammatory cytokines.

We next tested whether s.c. injection of cM362-139(IVT) plus OVA induced CTL proliferation. The OVA tetramer assay and IFN-γ production were employed to evaluate OVA-specific CD8$^+$ T-cell activation. Combination therapy of cM362-139(IVT) with OVA exhibited an increase in the frequency of Ag-specific CD8$^+$ T cells comparable to poly(I:C) with OVA (Fig. 4b). Ag-specific CD8$^+$ T cells clonally proliferated against EG7 as *in vitro* cytotoxicity was directed exclusively to EG7 in mice stimulated with cM362-139(IVT) with OVA (Fig. 4c) as well as poly(I:C) with OVA[9]. EG7 growth retardation by cM362-139(IVT) with OVA was largely abrogated in TLR3 KO mice (Supplementary Fig. 8), suggesting that cM362-139(IVT) acts on host TLR3 *in vivo*. However, mild tumour growth retardation was still observed with cM362-139(IVT) with OVA in TLR3 KO mice (Supplementary Fig. 8), implying minor involvement of EG7 cell TLR3 or other host RNA sensors, such as RLR[26] and DEAD-box helicases[27], in *in vivo* tumour regression. Yet, tumor cell's TLR3 signaling and chemokine induction might affect tumor remission (refs 28–30).

We finally tested whether chemically synthesized cM362-140 harbours the ability to retard EG7 growth in the same model. The synthetic cM362-140 showed ~80% activity for IFN-β reporter activation compared with cM362-139(IVT) and a single